Earth's mantle composition revealed by mantle plumes

Dominique Weis, Karen S. Harpp, Lauren N. Harrison, Maud Boyet, Catherine Chauvel, Cinzia G. Farnetani, Valerie A. Finlayson, Kanani K. M. Lee, Rita Parai, Anat Shahar, et al.

The Composition of the Earth's Mantle Revealed by Mantle Plumes

Weis[1*], Dominique; Harpp[2], Karen; Harrison[3], Lauren N.; Boyet[4], Maud; Chauvel[5], Catherine; Farnetani[6], Cinzia G.; Finlayson[7], Valérie A.; Lee[8], Kanani K.M.; Parai[9], Rita; Shahar[10], Anat; Williamson[11], Nicole B.

* Corresponding author

1. Department of Earth, Ocean and Atmospheric Sciences, University of British Columbia 2020-2207 Main Mall, Vancouver, BC, V6T-1Z4, Canada – dweis@mail.ubc.ca

2. Department of Earth and Environmental Sciences, Colgate University, Hamilton, NY 13346, USA - kharpp@colgate.edu

3. U.S. Geological Survey, 345 Middlefield Road, Menlo Park, CA 94025, USA - lnharrison@usgs.gov

4. Université Clermont Auvergne, CNRS, IRD, OPGC, Laboratoire Magmas et Volcans, F-63000 Clermont-Ferrand, France - maud.boyet@uca.fr

5. Université Paris Cité, Institut de Physique du Globe de Paris, CNRS, 1 rue Jussieu Paris 75005, France - chauvel@ipgp.fr

6. Université Paris Cité, Institut de Physique du Globe de Paris, CNRS, 1 rue Jussieu Paris 75005, France - cinzia@ipgp.fr

7. Department of Geology, 8000 Regents Drive, University of Maryland, College Park, MD 20742, USA - vfinlays@umd.edu

8. Physics Department, U.S. Coast Guard Academy, 208 Smith Hall, 31 Mohegan Avenue New London, CT 06320, USA - kanani.km.lee@uscga.edu

9. Department of Earth and Planetary Sciences, Washington University in St. Louis, 1 Brookings Drive, Saint Louis, MO 63130, USA - parai@wustl.edu

10. Earth and Planets Laboratory, Carnegie Institution for Science, 5241 Broad Branch Rd. N.W., Washington, DC 20015, USA - ashahar@carnegiescience.edu

11. Department of Earth, Ocean and Atmospheric Sciences, University of British Columbia 2020-2207 Main Mall, Vancouver, BC, V6T-1Z4, Canada – nwilliam@eoas.ubc.ca

Abstract

Earth's mantle is integral to many processes that shape our planet, including convection, crustal formation, crustal recycling, and global heat and volatile budgets. Still, many questions remain unresolved about mantle composition and its influence on geodynamics today and throughout geologic time. Because they originate at depths that can extend to the core-mantle boundary, mantle plumes provide invaluable information about the composition of the deep mantle. In this review, we discuss the effectiveness and challenges of using isotopic analyses of plume-derived rocks to document the origin and composition of mantle heterogeneities, early-formed mantle reservoirs, crustal recycling processes, core-mantle interactions, and mantle evolution. We discuss isotopic methods and improvements to existing isotopic systems to characterize plume-derived ocean island basalts. Nevertheless, because mantle plumes vary in many properties, including magmatic flux, temperature, tectonic environment, and compositions, geochemical observations on plume-generated systems must be considered carefully before making interpretations about Earth's interior. Consequently, plumes and their melts should be evaluated along a spectrum that acknowledges and contextualizes their differences, particularly mantle flux. Ultimately, the most important advancements in mantle geochemistry, architecture, and dynamics will emerge from cross-disciplinary studies in diverse fields such as experimental petrology, mineral physics, numerical geodynamics, seismology, and geochemistry.

Section 1 Introduction

The mantle plays a critical role in many of Earth's most dynamic systems. At 84% of Earth's volume, the mantle is the source of mid-ocean ridge, convergent margin, and intraplate volcanism, processes integral to forming and recycling oceanic and continental crust (White, 1985; Zindler and Hart, 1986; Hofmann, 1997; 2003; Labrosse et al., 2007; White, 2015). The mantle also contributes to Earth's water and heat budgets via radioactive decay and thermochemical convection. In the lower mantle (660-2890 km depth), seismic wave velocity variations reflect differences in temperature and/or composition (Davies and Davies, 2009; Tkalčić et al., 2015; Garnero, 2000; Koelemejier et al., 2016; Ritsema and Lekic, 2020), suggesting that the lower mantle, or part of it, is a reservoir for compositionally distinct material, including recycled and potentially ancient primitive components. Thus, understanding many fundamental Earth processes relies on documenting the composition and spatial heterogeneity of Earth's mantle today and its evolution throughout geologic time.

At shallow mantle depths (<100 km) below spreading ridges, upwelling causes the upper mantle to melt via adiabatic decompression. These processes generate mid-ocean ridge basalts (MORB), which provide insight into the composition of the upper mantle (e.g., Gale et al., 2013 and references therein). By contrast, mantle plumes provide invaluable insight into the geochemistry of Earth's deeper interior and occur in all tectonic settings (Fig. 1a). They originate at different depths, from shallow upwellings in the upper mantle (Duvernay et al., 2021) to deeply sourced plumes (Courtillot et al., 2003) that rise from near the core-mantle boundary (CMB) at ~2800 km. Above 1000 km (French and Romanowicz, 2015), mantle plumes form narrow, roughly cylindrical pipes of anomalously hot mantle that upwell and partially melt to form ocean island basalts (OIBs) on oceanic plates. Mantle plume melting occurs at sublithospheric depths, requiring a mantle source that is either hotter than the upper mantle, or enriched in rocks and/or fluids that lower the solidus temperature. Thus, mantle plumes provide the heat and components necessary for intraplate magmatism and to generate OIBs (Fig. 1b). Plume-generated oceanic

islands usually sample the mantle without chemical interference from the continental crust or subcontinental lithospheric mantle, providing a unique geochemical window into the composition of Earth's mantle and its evolution over time, including the sources of deeply rooted plumes.

In this review, we discuss developments in the isotopic analysis of mantle plume-fed ocean island basalts, an essential tool for documenting mantle heterogeneity (Fig. 1b). An NREE review by Koppers et al. (2021) discusses progress in seismic imaging, mantle flow modelling, plate tectonic reconstructions, and geochemical analyses of deep mantle plumes and their roles in Earth processes. Our review, which complements that of Koppers et al. (2021), focuses on the geochemistry and geodynamics of deep plumes that form well-studied oceanic islands (e.g., Hawai'i, Réunion, Kerguelen, and Galápagos, among others). New perspectives on the geochemical composition of the mantle have recently been developed from advancements in analytical techniques and novel isotopic systems, allowing the resolution of smaller isotopic variations in OIB samples. These new techniques and isotopic systems shed light on the presence, source, and age of heterogeneities in the deep mantle. We present a comprehensive perspective on enduring paradigms and new advances in mantle geochemistry, as well as insights that the geochemistry of ocean island basalt provides toward understanding Earth's evolution.

Section 2 Fundamentals of Mantle Plumes

The strength of a plume's upwelling flux, its composition, and the duration of its activity have been used to classify plumes (Courtillot et al., 2003; Jackson et al., 2018; Koppers et al., 2021; Fig. 1a). Primary plumes have a seismic velocity anomaly of at least -1.5% between 1,000 and 2,800 km depth (extending to the CMB), a linear and age-progressive volcanic chain, a large igneous province (LIP) at the oldest end of the volcanic chain, a strong magmatic flux, and high $^{3}He/^{4}He$ or other indications of compositions distinct from those of mid-ocean ridge basalts (Courtillot et al., 2003; Montelli et al., 2006; Boschi et al., 2007; King and Adam, 2014; French and Romanowicz, 2015).

Seismic tomography and geodynamical studies suggest that most OIB-generating volcanoes are produced by plumes that originate along the edges of Large Low Shear Velocity Provinces (LLSVP), commonly interpreted as thermochemical piles at the CMB (Burke and Torsvik 2004; Thorne and Garnero, 2004; Torsvik et al., 2006; Burke et al., 2008; Doubrovine et al., 2016; Garnero et al., 2016). Early geodynamical models explored ancient, accumulated recycled crust as the LLSVP source (e.g., Christensen and Hofmann, 1994; Brandenburg et al., 2008), whereas more recent models focus on the interplay between the recycled crust and a layer of primordial iron-rich material with an excess density of about 1% (e.g., Li, et al. 2014; Williams et al., 2015; Nakagawa and Tackley, 2014; Jones et al., 2021). Alternatively, dense and reduced mantle material may pool at the CMB, contributing to the formation of LLSVPs (Gu et al., 2016). Laboratory experiments (Davaille, 1999; Limare et al., 2015) and numerical simulations successfully reproduce the formation of large thermo-chemical plumes observed in recent tomographic models (French and Romanowicz, 2014). In some models, both the LLSVP and the ambient mantle supply material to plumes rising from the boundary between them (Fourel et al., 2017).

Also detected at the core-mantle boundary, Ultra-Low Velocity Zones (ULVZs) are characterized by strong S-wave (~30%) and P-wave velocity reduction (10%), best explained by a ~10% density increase (Thorne and Garnero, 2004; McNamara, 2019 and references therein). The ULVZs are discrete areas 10-40 km high that extend laterally for up to ~1000 km along the core-mantle boundary (Cottaar and Romanowicz, 2012). Models for the origin of ULVZs include core-mantle reactions (Knittle and Jeanloz, 1989), the presence of dense silicate melt (Williams and Garnero, 1996), relics of banded iron formations subducted 2-3 Ga ago (Dobson and Brodholt, 2005), or zones of iron-enriched post-perovskite (Mao et al., 2006). Of importance to mantle geochemistry is the possibility that ULVZs host geochemical signatures distinct from the rest of the mantle, including some that may record early differentiation or diffusion across the core-mantle boundary (e.g., Mundl-Petermeier et al., 2020; Yoshino et al., 2020). The high density of ULVZs inhibits their convective stirring, and only the most vigorous plumes may entrain thin tendrils of ULVZ material by viscous coupling (i.e., Williams et al., 2015).

Mineral physics research has explored ways that mantle heterogeneity can be expressed through phase relations, density, and elastic moduli variations due to changes in bulk composition (e.g., Lee et al., 2004; Ricolleau et al., 2010; Dorfman et al., 2013), water content (e.g., Litasov and Ohtani, 2007; Zhou et al., 2022), and differences in redox state (e.g., Gu et al., 2016, Creasy et al., 2020). While accessory phases can vary in type and abundance, the dominant phase in the lower mantle is bridgmanite, a Mg-silicate perovskite (Tschauner et al., 2014). The strength of bridgmanite's structure may encourage the formation of narrow channels of upwelling and downwelling, thereby stabilizing deep-rooted mantle upwellings from near the core-mantle boundary (Ballmer et al., 2017).

Geochemical research on mantle plumes reveals complex spatial variations in OIBs (Text Box #1; Fig. 2). The best-studied example is Hawai'i, where the distinct isotopic compositions of Loa- and Kea-trend volcanoes indicate a bilateral compositional asymmetry, or compositional "stripes" in the plume (Abouchami et al., 2005). Specifically, the southwestern Loa chain consists of more enriched material, and the northeastern Kea chain has more depleted signatures. Weis et al. (2011) proposed that the Loa chain is sourced in the Pacific LLSVP and Kea lavas are supplied by the ambient lower mantle (Nobre-Silva et al., 2013a; Williamson et al., 2019), a reflection of the plume's location along the northern boundary of the Pacific LLSVP. The compositionally distinct materials from the LLSVP and the lower mantle only mix minimally between the CMB and the surface, where they are expressed as distinct signatures in erupted lavas (Kerr and Mériaux, 2004; Farnetani and Hofmann, 2009; Weis et al., 2011). Notably, similar compositional patterns have been recognized in other LLSVP-sourced plumes, including the Samoan, Galápagos, Easter, and Marquesas Islands in the Pacific (Weis et al., 2011; Huang et al., 2011; Chauvel et al., 2012; Payne et al., 2013; Harpp et al., 2014; Harpp and Weis, 2020), and, in the Atlantic at the western edge of the African LLSVP, Tristan and Gough (Rohde et al., 2013).

This new paradigm for plume origins (Weis et al., 2011) has led to additional nuances and proposals for plume models as well. In the Marquesas, the sizes of the heterogeneities appear to be smaller than in Hawai'i, potentially originating from within the plume itself instead of the LLSVP-lower mantle boundary (Chauvel et al., 2012). Harrison et al. (2017) suggest that rather than originating at the LLSVP-mantle interface, a drifting Hawaiian plume gets anchored on the

LLSVP, resulting in the entrainment of LLSVP material; this model helps explain the abrupt increase in plume flux along the chain after the bend. Finally, modelling results from Jones et al. (2017) propose that the compositional zonation in Hawai‘i reflects a response to a major change in absolute plate motion.

Buoyancy Flux of Plumes

The strength, or buoyancy flux, of a mantle plume influences the partial melting regime of its corresponding oceanic island system (e.g., Schilling, 1991). Tholeiitic and alkalic basalts are produced, respectively, by higher or lower degrees of partial melting. Thus, whether tholeiitic or alkalic basalts dominate an oceanic island provides insight into the buoyancy flux and the mantle potential temperature of a plume system. For example, the Hawaiian chain represents a rare occurrence of high-volume magmatism that produces tholeiitic basalts; other examples include Réunion, Iceland, Galápagos, and Easter Islands (e.g., Sleep, 1990; King and Adam, 2014). These systems also have elevated buoyancy flux and/or mantle potential temperature (Schilling, 1991; White et al., 1993; Kingsley et al., 1998; 2007; Jackson and Dasgupta, 2008; Jackson et al., 2017). Iceland is distinct as the only oceanic island that follows a silica-saturated tholeiitic evolution trend (Supplementary Fig. a; Gale et al., 2013). Alkalic lavas, formed from lower degrees of partial melting, dominate some plumes with intermediate fluxes, such as the Cook-Austral chain (Jackson et al., 2020b) and Society Islands (Duncan et al., 1986) (Fig. 1a). Generally, however, most intraplate oceanic volcanoes produce dominantly alkalic melts (Haase et al., 2019), suggesting that high-degree partial melting of some mantle plumes may be uncommon, at least during the Cenozoic.

Furthermore, plume strength may be enhanced by proximity to an LLSVP, as proposed for Hawai‘i (Harrison et al., 2017; Harrison and Weis, 2018). The volume of magma produced along the Hawaiian chain has increased over the last 45 Myr, in contrast to the trend predicted by mantle plume models (e.g., Wessel, 2016; Weis et al., 2020). Moreover, the highest-flux plumes, including Hawai‘i, overlie “mega-ULVZ” structures at the CMB (Cottaar and Romanowicz, 2012), implying links between lower mantle structures, the strength of a plume, its temperature, and its melting conditions (Harrison et al., 2017).

Influence of Plate Motion and Plate Boundaries

A plume’s compositional structure will be recorded by its volcanoes in different ways depending on lithospheric thickness, proximity to a spreading ridge, plate motion vectors, and the geometry of the compositional structure within the plume conduit itself. Lithospheric thickness can influence the depth and degree of melting, spreading ridges can re-direct upper mantle flow, and the direction of plate motion relative to the compositional cross-section of the plume will dictate how plume compositions are expressed at the surface. As an example of the latter case, since ~3-6 Ma at Hawai‘i, both the LLSVP boundary and current Pacific plate motion vector (Wessel and Kroenke, 2009) are oriented along similar NW-trending strikes, forming the two parallel chains of compositionally distinct volcanoes (Weis et al., 2011; Farnetani et al., 2012). In the Galápagos, by contrast, the orientation of the LLSVP boundary is oblique to plate motion, resulting in early erupted, enriched material from the LLSVP being buried beneath younger, more depleted material from the ambient mantle (Harpp and Weis, 2020). In addition, shifts in plate motion direction might shear mantle plume stems and generate ephemeral changes in the spatial distribution of erupted, compositionally distinct material (e.g., Jones et al., 2017).

Plumes will interact with the adjacent spreading centers, causing plume material to be incorporated into the return flow of the ridge and enhancing entrainment of depleted upper mantle into plume-generated lavas as observed in the Azores, Galápagos, and Cretaceous Hawaiian systems, among other near-ridge plumes (e.g., White et al., 1993; Harpp and White, 2001; Harrison et al., 2020). The near-zero lithospheric thickness of ridge-proximal plumes may also increase plume melting and affect the magmatic architecture of ocean islands formed near the ridge (e.g., Weis and Frey, 2002; Regelous et al., 2003; Harpp and Geist, 2018;). Near-ridge plumes, including Iceland, Galápagos, Kerguelen, and Easter produce abundant tholeiitic lavas that require higher degrees of partial melting than other mantle plumes (White et al., 1993; Kingsley et al., 1998, 2007; Ito et al., 1996; Schilling, 1991; Weis and Frey, 2002). In plumes near subduction zones, additional crustal flexure of the plate may generate melt and/or encourage entrainment of upper mantle material, as proposed for Samoa (Konter and Jackson, 2012; Jackson et al., 2014) and for volcanism that cannot be plume-related in the Emperor Seamounts near the Aleutian Arc (e.g., Kerr et al., 2005).

Section 3 Oceanic Island Volcanism

Owing to the lack of interaction with continental material, ocean islands with deep plume sources provide the most direct view and accurate representation of lower mantle composition (e.g., Harrison et al., 2017; Weis et al., 2020).

OIB: Geochemical Overview

Oceanic island volcanoes feature a variety of volcanic rock types, including picro-basalts, rhyolites, basanites, phonolites, and trachytes (Supplementary Fig. a). Nevertheless, the dominant rock type is basalt. In this review, we focus on shield-stage basaltic magmas that form lavas of tholeiitic or alkalic composition because they have experienced the least differentiation and contamination en route to the surface. Another approach to studying mantle heterogeneity is to analyze melt inclusions. Such studies (e.g., Saal et al., 2005; Stracke et al., 2019) detect greater isotope heterogeneity than is observed in bulk analysis of erupted lavas. Melt inclusions sample geochemical variations on a much smaller scale (20-30 μm), capturing different aspects of the magmatic system. They represent a "snapshot" of melt pockets prior to melt amalgamation, magma mixing, and significant fractional crystallization than whole rock OIB analyses. Melt inclusion analyses are challenging analytically and vulnerable to many processes that disturb or distort their compositions post-entrapment, generating data with lower precision because of their small size. This review focuses exclusively on isotopic analyses in rock samples that integrate melts generated by many cubic kilometres of the mantle source (Rudge et al., 2013) (see Text Boxes 2 & 3).

To some extent, the compositional diversity of ocean island basalts (especially compared to the relative homogeneity of mid-ocean ridge basalts; Hofmann, 1997; Gale et al., 2013) reflects the lower degrees of partial melting of OIBs compared to MORBs. That said, melting systematics can only explain a small fraction of the observed variations (Hofmann, 1997; White, 2010). Characteristic features of major and trace element compositional variations in OIB include enrichment in the light rare earth elements (REEs) compared to the primitive mantle (which refers to the composition of Earth's mantle soon after core formation), depletion in heavy REEs relative to middle and light REEs, and near-constant ratios of the most incompatible elements (left side of Supplementary Fig. b; Hofmann et al., 1986; Newsom et al., 1986;

Willbold and Stracke, 2006). Their rare earth element systematics suggest that most OIB melts are generated primarily in the garnet stability field (>80 km depth), which reflects the higher mantle temperatures of plumes (e.g., Gast, 1968). In contrast, most MORBs begin melting at shallower levels where garnet is no longer stable, resulting in no significant middle to heavy REE fractionation in the generated magmas.

In some cases, major element oxides and trace element concentrations correlate with the dominant isotopic trends displayed by OIBs (Jackson and Dasgupta, 2008; Jackson et al., 2012), which is notable because variations in major and trace elements are typically generated by different processes (e.g., degree of melting, magmatic differentiation) than are variations in isotopic compositions (e.g., compositional differences in time-integrated mantle sources). Thus, correlations between major and trace elements and isotopic compositions in OIB may reflect mixtures of compositionally-distinct sources melting to variable extents and/or the fact that the compositionally distinct materials in the mantle differ in their major and trace element signatures as well as their isotopic compositions (Rudge et al., 2013).

OIB Isotopic Mantle End-members

Radiogenic isotope ratios in ocean island lavas vary within a field constrained by a minimum of four end-member isotopic compositions (HIMU, EM-I, EM-II, and DMM, Depleted MORB Mantle; White, 1985; Zindler and Hart, 1986; Hart et al., 1992; Hofmann, 1997; Fig. 2a-d). Most ocean island chains define mixing arrays in bivariate isotope plots that extend between one of the three end-member compositions and a single, focal area within the mantle isotopic field in Sr-Nd-Pb(-Hf) isotopic space (Fig. 2 and Supplementary Figs. f-i; e.g., Zindler et al., 1982; White, 1985; Zindler and Hart, 1986; Hart et al., 1992; Stracke et al., 2005; White, 2015). The focal area is proposed to be a fifth composition, variably named PREMA (PREvalent MAntle; Zindler and Hart, 1986), FOZO (Focus Zone; Hart et al., 1992), C (Common component; Hanan and Graham, 1996), or PHEM (Primitive HElium Mantle; Farley et al., 1992) depending on the authors (Fig. 3 inset).

The five compositional end-members define the range of isotopic compositions in OIB, and thus in the mantle sampled by plumes. Except for PREMA, these end-members are chemically and isotopically distinct from each other and thought to come from separate chemical reservoirs in the mantle, resulting from processes that generate unique chemical signatures and evolve over time. Below, we consider the geochemical signatures of these mantle reservoirs (Supplementary Table 1), their origins, and the insights they provide into the composition and evolution of the mantle.

The HIMU Endmember

The HIMU mantle end-member is named for its high U/Pb (μ) source ratio (Zindler and Hart, 1986). The extreme U/Pb ratios required to generate HIMU Pb isotopic signatures (Fig. 2a) indicate that the original mantle source had high initial U/Pb (μ) and Th/Pb (ω) (Chauvel et al., 1992). The most commonly invoked mechanism to explain the removal of Pb required for the HIMU signature is dehydration of ancient, subducted oceanic crust, followed by storage in the mantle for 1.5-2 billion years prior to incorporation into mantle plumes (Hofmann and White, 1982; White, 1985; Zindler and Hart, 1986; Chauvel et al., 1992, 1997; Stracke et al., 2005; Kelley et al., 2005). Alternative explanations include contributions to the plume source of

carbonatitic silicate melts from recycled oceanic crust (Dasgupta et al., 2007; Jackson and Dasgupta, 2008), ancient carbonate-metasomatized sub-continental lithospheric mantle (Weiss et al., 2016; Homrighausen et al., 2018), and recycled Archean marine carbonates (Castillo, 2015). Of the major mantle end-members sampled by plumes, HIMU has limited distribution, is the least voluminous (Figs. 1 & 3), and is the dominant component in only a few small ocean islands (Cook-Austral, St. Helena, Mangai, Tubuai, Rurutu).

The Enriched Mantle (EM-I and EM-II) End-members

On the basis of OIB isotopic systematics, Zindler and Hart (1986) identified two distinct enriched mantle end-members (EM-I and EM-II). The EM-I end-member may originate from recycling of delaminated subcontinental lithosphere and/or from subducted pelagic sediments or Archean carbonates into the deep mantle (Hoffman and White, 1982; Weis et al., 1989; Chauvel et al, 1992; Blichert-Toft et al., 1999; Eisele et al., 2002; Garapić et al., 2015; Delavault et al., 2016; Wang et al., 2018; Boyet et al., 2019; Cordier et al., 2021), but there is little consensus about its origin. By contrast, the EM-II reservoir exhibits contributions from materials once present on continents (Zindler and Hart, 1986; Weaver, 1991; Chauvel et al., 1992; White and Duncan, 1996; Jackson et al., 2007; Jackson and Dasgupta, 2008), although alternative models have been proposed, including the incorporation of ancient metasomatized oceanic lithosphere into the EM-II reservoir (Workman et al., 2004). The EM-I (Kerguelen, Heard, Pitcairn, Tristan-Gough, Hawai‘i) and EM-II (Marquesas, Society, Samoan Islands) end-members dominate OIB-producing systems and are important contributors to the buoyancy flux of many plumes (Figs. 1 & 3).

The Prevalent Mantle (PREMA)

Most OIB isotopic arrays, especially major mantle plumes highlighted here, have one end anchored at the center of the global isotopic OIB data field, the intermediate area defined as PREMA (Zindler and Hart 1986). The PREMA reservoir represents the average ambient lower mantle (Figs. 2 & 3 inset) and is compositionally distinct from the upper mantle. The high $^{3}He/^{4}He$ ratios relative to MORB (Hanan and Graham, 1996) suggest that PREMA samples a less degassed reservoir than other parts of the mantle (Class and Goldstein, 2005; Gonnermann and Mukhopadhyay, 2009). PREMA may represent primitive mantle if that reservoir has non-chondritic Sm/Nd, Nb/U, and Ce/Pb (Nobre-Silva et al., 2013a; White, 2015, Hofmann et al., 2022). Alternatively, the PREMA reservoir could be a well-mixed combination of a less-processed, less-degassed mantle with recycled components (Zindler and Hart, 1986; Stracke et al., 2006; Parai et al., 2019). Hawai‘i, Iceland, and the Galápagos exhibit substantial PREMA contributions (Nobre-Silva et al., 2013a; Harpp and Weis, 2020).

The Depleted Mantle Source in OIBs

The major and trace element characteristics of strongly depleted OIB lavas (Supplementary Figs. a-e) are consistent with a mantle source that has a long-term history of melt extraction and, therefore, depletion in the most incompatible trace elements (Salters and Stracke, 2004). The depleted component in OIBs, although easily masked by mixing with melts from enriched heterogeneities in the mantle source, has been shown to be a component of some Azores lavas, as evidenced by analysis of melt inclusions that record contributions from depleted melts prior to magma mixing and homogenization (Genske et al., 2019). Rare, depleted signatures in Hawaiian lavas and xenoliths also support a depleted component in mantle plumes

(Frey et al., 2005; Bizimis et al., 2005; DeFelice et al., 2019). In Iceland, the Azores, and the Galápagos, the depleted signature is attributed to their near-ridge settings, where higher degrees of mantle melting occur under a thin lithosphere (e.g., White et al., 1976; Schilling et al., 1982; Humphris et al., 1985; Hart et al., 1992; Moreira et al., 1999; Harpp and Weis, 2020).

Uncertainty persists regarding the origin of depleted mantle compositions in OIB (Hart et al., 1992; Harrison et al., 2020; Stracke et al, 2022) and whether these compositions: 1) comprise a large proportion of the lower mantle and, therefore, if either the DMM or an early-enriched reservoir is a major matrix component in mantle plumes (Hofmann et al., 2022); 2) represent melting of an entrained sheath of upper depleted mantle material; and/or 3) reflect large degrees of melting of the plume source, as expected underneath thin lithosphere. In contrast to this prevailing view of mantle components, a recent multi-variate statistical data analysis suggests that the apparent overlap of MORB-OIB data trends in 2D isotope ratio diagrams does not translate consistently to multi-dimensional isotope data space, leading to the proposal that compositional variations displayed by MORB-OIB are controlled by smaller-scale, regional domains, rather than a limited number of global-scale reservoirs (Stracke et al., 2022). Such major differences in interpretation about the magnitude and dynamics of compositional reservoirs highlights the need for a more nuanced understanding of these important parts of the mantle and their roles in mantle plumes.

Section 4 Subduction and Mantle Heterogeneity

Early in the development of mantle plume theory, plumes were thought to be supplied exclusively by the primitive lower mantle and depleted upper mantle (Allègre, 1982). Primarily on the basis of geochemical data, the radical idea that the source of ocean island basalts might contain ancient oceanic crust was proposed in the 1980s (Hofmann and White, 1982). This hypothesis posits that oceanic plates are recycled via subduction into the lower mantle, where they are subsequently sampled by plumes; this cycle of downwelling and upwelling provided a critical step forward for understanding mantle plumes and their role in the global plate tectonic system. Geochemical evidence confirms the contribution of recycled oceanic crust to ocean island mantle sources (White, 1985; Zindler and Hart, 1986; Chauvel et al., 1992, 1997; Stracke et al., 2005; Kelley et al., 2005). Moreover, seismic data (Fukao and Obayashi, 2013) and geodynamic models (Jones et al., 2021) document the transport of subducted plates to the lower mantle.

The recycled oceanic crust consists of various materials, including basaltic crust and the overlying sedimentary pile (Fig. 1b). Whereas basaltic crust has a chemical composition that is, within an enrichment factor, not significantly different from its upper mantle source, the composition of sedimentary material can be highly diverse. The average composition for global subducting sediment (GLOSS; Plank and Langmuir, 1998) is similar to continental crust but chemically distinct from the mantle or basaltic material; thus, even minuscule contributions of sediment to the source of ocean island basalts can be detected using geochemical methods. Atmospheric and spallation-generated ^{10}Be concentrations, lithium, boron, and iron isotope compositions, as well as U-series disequilibrium studies have demonstrated that sediments survive subduction processing to mantle depths (Morris et al., 2002; Turner et al., 2003; Deschamps et al., 2010; Tang et al., 2014; Smith et al., 2021), confirming that their inclusion in the mantle plume source is a viable model. Consequently, to understand mantle plumes and their

sources fully, it is essential to document the geochemical composition of the subducted oceanic crust and the associated sediments transported into the lower mantle.

Recycled Material in Ocean Island Basalts

As sediment and oceanic crust are subducted into the mantle, they undergo distinct compositional changes. Specifically, subducted material is dehydrated or melts and it loses a large proportion of the fluid-mobile elements (e.g., Li, B, Cs), while retaining much of the more refractory elements (e.g., REE, HFSE; Porter and White, 2009; Ryan and Chauvel, 2014; Turner and Langmuir, 2022), making it possible to identify and quantify the contributions of recycled oceanic crust and sediment to mantle sources (e.g., Chauvel et al., 2008; Porter and White, 2009).

In particular, the presence of sediments in the OIB source has been posited to explain some of the specific trace element characteristics of EM-I and EM-II basalts. The two canonical ratios, Ce/Pb and Nb/U, have generally constant values in all mantle-derived magmas (25 ± 5 for Ce/Pb and 47 ± 10 for Nb/U; Hofmann et al., 1986; Hofmann et al., 2022); in EM-I and EM-II OIBs (Supplementary Fig. d), these ratios deviate from their universal mantle values toward lower ones typical of continental crust (3.7 for Ce/Pb and 4.4 for Nb/U; Chauvel et al.,1992; White and Duncan, 1996; Rudnick and Gao, 2003; Jackson et al., 2007; Cordier et al., 2021), providing some constraint on the origin of isotopic enrichment in the OIB source.

Radiogenic isotopes are even more effective than trace elements at detecting and quantifying sedimentary material in OIB sources. For example, 6% sediment in the mantle source shifts the Sr isotopic composition of Samoan basalts from 0.704 to elevated values (~0.720) not measured in any other OIB (Jackson et al., 2007). Most EM-II basalts have significantly less radiogenic Sr isotope ratios than those in Samoan lavas, corresponding to a sediment contribution of <2% to their sources. Nevertheless, the community agrees that most OIBs with radiogenic Sr coupled to unradiogenic Nd and Hf must originate from a source containing some recycled sedimentary material (Stracke, 2012).

The most commonly invoked model to explain the combination of unradiogenic Sr isotopic ratios with highly radiogenic Pb isotopic signatures, as documented in HIMU basalts (Fig. 2d and Supplemental Fig. i), is the presence in the source of old (~2 Ga) oceanic crust that lost some of its Pb during subduction. This interpretation is supported by the elevated Ce/Pb of most HIMU basalts (typically >30; Cordier et al., 2021), which reflects the loss of Pb to subduction fluids. Furthermore, the relationship between Nd and Hf isotope ratios in ocean island basalts (Fig. 2c and Supplemental Fig. h) requires contributions from both recycled basalts and sediments with ages ranging from Archean to present-day (Vervoort et al., 1999; Blichert-Toft et al., 1999; Chauvel et al., 2008).

Heavy noble gas (Ne, Ar, Kr, Xe) isotope ratios in mantle rocks are also sensitive tracers of subducted material. Atmospheric heavy noble gases, which have distinctive elemental ratios and isotopic compositions, are incorporated into the mantle through subduction (Holland and Ballentine, 2006; Mukhopadhyay, 2012; Tucker et al., 2012; Parai et al., 2012; Péron et al., 2021; Parai, 2022), though this “regassing” transport was likely inefficient prior to 2.5 Ga (Parai and Mukhopadhyay, 2018; Péron and Moreira, 2018). Once corrected for shallow post-eruptive

atmospheric contamination, the Xe isotopic signatures of OIB mantle sources are dominated by regassed atmospheric Xe (Parai et al., 2019). This is an unambiguous indication of surface-derived material in the OIB mantle source, because the atmospheric Xe isotopic signature reflects sources and processes distinct from mantle Xe (Caffee et al., 1999; Avice and Marty, 2020). Likewise, Kr isotopes in Iceland and Galápagos samples indicate strong regassing of atmospheric Kr (Péron et al., 2021). Regassed atmospheric signatures are present even in samples with high $^{3}He/^{4}He$ and primitive, solar-like Ne isotopes (Mukhopadhyay, 2012; Pető et al., 2013; Péron et al., 2021).

The oceanic crust also carries distinctive signatures from the surface into the mantle. For example, lithium (Li) is incorporated into oceanic crust during hydrothermal alteration and serpentinization. Of the stable isotope systems commonly used in the geosciences, Li has the largest relative mass difference between its two isotopes (^{6}Li and ^{7}Li). As such, low temperature, aqueous processes result in extreme fractionation (Tomascak, 2004; Tang et al., 2014; Penniston-Dorland et al., 2017) and, consequently, Li isotopes are useful tracers of processes that involve fluid mobilization, such as subduction (Fig. 4). During the subduction process, Li is transported to the mantle wedge as oceanic slabs are dewatered and metamorphosed (Bouman et al., 2004; Deschamps et al., 2010). Lithium isotopic values consistent with subduction alteration have been measured in some OIBs from Hawai‘i, Cook-Austral, St. Helena, and Azores (Chen and Frey, 2003; Vlastélic et al., 2009; Krienitz et al., 2012; Harrison et al., 2015), providing evidence for the recycling of subduction-altered material into the OIB source. By contrast, MORBs exhibit a relatively uniform Li isotopic composition ($\delta^{7}Li = 3.5 \pm 1.0‰$; Marschall et al., 2017; Penniston-Dorland et al., 2017). There is also a measurable difference between Li isotopic compositions of HIMU OIB ($\delta^{7}Li = 2.5\text{-}8.5‰$) and EM-I OIB ($\delta^{7}Li = 0.5\text{-}4.5‰$), which likely reflects the diversity of subducted components that contribute to these mantle reservoirs (Krienitz et al., 2012; Harrison et al., 2015).

The type of subducted surface material present in OIB sources is best estimated using isotopic systems with large natural fractionations. For example, stable isotopes of thallium (^{205}Tl and ^{203}Tl) are fractionated up to 35 epsilon units, and exhibit large concentration contrasts between geochemical reservoirs (e.g., pelagic sediments: $\varepsilon^{205}Tl$ and [Tl] up to +5 and 1000 ng/g (Rehkämper et al., 2002); low-temperature altered oceanic crust: $\varepsilon^{205}Tl$ and [Tl] as low as -15 and 5-50 ng/g (Nielsen et al., 2006a); mantle: $\varepsilon^{205}Tl$ of -2 ± 0.5 and <1 ng/g Tl (Nielsen et al., 2017). Ocean island basalts exhibit a wide range of $\varepsilon^{205}Tl$ values (-6.4 to +6.6; Brett et al., 2021). Heavy $\varepsilon^{205}Tl$ (up to +4) in Hawaiian tholeiites have been attributed to recycled subducted sediment in the plume source (Nielsen et al., 2006b; Williamson et al., 2021), potentially sampled from the ambient mantle on the periphery of the Pacific LLSVP (Williamson et al., 2021). Conversely, light $\varepsilon^{205}Tl$ (down to -10) in lavas from St. Helena may be traced to altered oceanic crust in their source and in the HIMU mantle reservoir (Blusztajn et al., 2018). In some cases, however, the Tl isotopic composition of OIB is ambiguous, requiring careful consideration when interpreting results and using this isotopic system as a mantle tracer (Brett et al., 2021; Williamson et al., 2021).

Finally, subducted material carries with it information about previous redox conditions at Earth's surface. In specific circumstances, such as the extreme surface conditions during the Archean prior to the Great Oxygenation Event at ~2.5-2.4 Ga (Farquhar et al., 2007), mass-

independent fractionation of stable isotopes such as sulfur (S) can occur. These signatures are then incorporated into sedimentary materials and basalts at the surface. For example, negative S isotopic anomalies have been detected in lavas from Mangaia (Cabral et al., 2013; Dottin III et al., 2020) and in basalts from Pitcairn (Delavault et al., 2016), which indicate that the HIMU (Mangaia) and EM-I (Pitcairn) mantle sources include material that was present at Earth's surface during the Archean, either in the form of Archean basaltic crust for Mangaia or Archean sedimentary material for Pitcairn.

New isotopic tracers continue to be developed that enable the characterization of recycled material in the OIB mantle source. For example, cerium (Ce) is redox-sensitive (Elderfield, 1988). Therefore, the measurement of the long-lived ^{138}La-^{138}Ce system may constrain the timing of pelagic sediment recycling into the mantle because no Ce anomalies are expected in water columns before the Great Oxygenation Event at ~2.5-2.4 Ga (Israel et al., 2020; Boyet et al., 2021). Collectively, a wide array of isotopic and trace element systems (see Text Box #2, Fig. 1b; Supplementary Figs. b-e) indicate that material previously at the surface of the Earth is present in the source of OIBs. That said, all isotopic characteristics of OIB cannot be explained only by recycling surficial material into the plume source; additional types of material must be present and the influence of several large-scale processes needs to be considered as well, including the physical proximity of plumes to LLSVPs, the depth and source of plume magmatism, and core-mantle interactions.

Section 5 Early-Formed Reservoirs

The OIB mantle source is a heterogeneous mixture of recycled surface materials, deep mantle material that separated early (>4.45 Ga) and experienced less degassing than the upper mantle, and potentially distinct remnant materials that formed early in Earth's history. Determining the age and the nature of early-formed materials is important for understanding the structure and dynamics of the lower mantle, especially given the spatial correlation of major mantle plumes with LLSVPs and ULVZs (e.g., Burke and Torsvik 2004; Torsvik et al., 2006; Doubrovine et al., 2016; Cottaar et al., 2022; see review by Hernlund and McNamara, 2015).

Tracing Early-Formed Reservoirs

Processes such as metal-silicate differentiation, magma ocean crystallization, and degassing of volatiles during energetic accretionary impacts influenced the geochemistry of early Earth's interior by fractionating groups of elements with different properties from each other. Because these events operated only for relatively short periods close to 4.5 Ga, the best tools to understand them and track their contributions to the OIB mantle are short-lived radionuclide systems, including ^{182}Hf-^{182}W, ^{146}Sm-^{142}Nd, ^{129}I-^{129}Xe, and ^{244}Pu-$^{131\text{-}136}$Xe, with half-lives between <10 Ma and ~100 Ma. Deviations in radiogenic products of some short-lived isotope systems (e.g., μ^{142}Nd and μ^{182}W) are small in OIBs (a few ppm), making their detection difficult (Fig. 5; e.g., Touboul et al., 2012b; Horan et al., 2018; see Text Box #3). Volatile elements pose additional challenges, owing to the loss of magmatic gas from samples and atmospheric contamination during and after eruption. Nevertheless, progress has been made measuring μ^{142}Nd, μ^{182}W, and ^{129}Xe/^{130}Xe variations in OIBs, as well as interpreting the significance of these anomalies for mantle history and dynamics.

Trace element abundances and ratios are also powerful tools for quantifying fractionation processes in the early Earth. For example, mass balance calculations using (Nb, Ta)/U and $^{143}Nd/^{144}Nd$ isotope ratios (Hofmann et al., 2022) demonstrate that continental crust and present-day depleted mantle could not have originated from the primitive mantle as previously thought (e.g., Jacobsen and Wasserburg, 1979; O'Nions et al., 1979; DePaolo, 1980). The measurements of a radiogenic excess of ^{142}Nd (+7.9 ± 1.9 ppm) in the mantle relative to its building blocks confirm this scenario (Frossard et al., 2022; Johnston et al., 2022). Therefore, the Earth's mantle may be slightly depleted in incompatible elements and characterized by higher Sm/Nd than chondrites. The Sm/Nd fractionation could be inherited from the accretion stage with the loss to space of enriched crusts formed in planetesimals by collisional (Frossard et al., 2022), removing the requirement for an early enriched reservoir to be preserved in the deep mantle (Boyet and Carlson, 2005).

Many stable isotope ratios of major elements may preserve early-formed isotopic signatures as well, because their values were not reset on a global scale (Text Box #2). Stable isotope fractionation has been constrained through high pressure-temperature experiments that simulate early differentiation events (e.g., Shahar et al., 2017) to predict the isotopic signatures in the OIB mantle source, providing potent clues about the characteristics of early-formed reservoirs.

Terrestrial Magma Ocean Relics

Small ^{142}Nd anomalies measured in a few OIB (-8 to +6 ppm; Fig. 5a) from Réunion (Peters et al., 2018) and Samoa (Horan et al., 2018) suggest that early-formed reservoirs may be preserved in the deepest part of the mantle. Owing to the short half-life of ^{146}Sm (~103 Ma), the variations measured in $^{142}Nd/^{144}Nd$ must reflect Sm/Nd fractionation that took place during the first few hundred million years of Earth history. Because both Sm and Nd are strongly lithophile rare earth elements and excluded from the metal phase during core-mantle differentiation (Faure et al., 2021), early fractionation of Sm/Nd must have occurred exclusively via silicate differentiation, providing evidence for crystallization of a terrestrial magma ocean. Most OIB are also characterized by negative ^{182}W anomalies (down to -25 ppm) (Mundl et al., 2017; Mundl-Petermeier et al., 2019; 2020; Peters et al., 2021), which may also represent the remnant of an early terrestrial magma ocean (Fig. 5b). However, core-mantle interaction could also affect the ^{182}W signal, making its interpretation ambiguous.

The short-lived ^{129}I-^{129}Xe system provides additional support for preservation of early-formed isotopic heterogeneity. Mantle Xe isotope compositions can be broken down mathematically into component contributions from accretion (chondritic Xe), radioactive decay, and atmospheric regassing (Caffee et al., 1999; Parai et al., 2019). Limited measurements of mantle-derived samples (from OIBs, MORBs, back-arc basin basalts, volcanic gases, and continental well gases) yield precise estimates of mantle source Xe compositions, corrected for shallow atmospheric contamination (Moreira et al., 1998; Mukhopadhyay, 2012; Parai et al., 2012; Tucker et al., 2012; Peto et al., 2013; Parai and Mukhopadhyay, 2015; Caracausi et al., 2016; Peron and Moreira, 2018; Bekaert et al., 2019; Parai and Mukhopadhyay, 2021; Peron et al., 2021). Ratios of $^{129}Xe/^{130}Xe$ (where ^{129}Xe is produced by decay of short-lived ^{129}I, and ^{130}Xe is not radiogenic) from Iceland, (Mukhopadhyay, 2012), the Rochambeau Rift in Samoa (Peto et al., 2013), and Galápagos (Péron et al., 2021) are low compared to the depleted mantle (Holland

and Ballentine, 2006; Tucker et al., 2012; Parai et al., 2012). Differential incorporation of atmospheric Xe with low $^{129}Xe/^{130}Xe$ into the OIB mantle cannot account for the OIB $^{129}Xe/^{130}Xe$ signatures (Fig. 5d). Thus, a low I/Xe ratio must have been established in the OIB mantle within the first ~100 Myr of Earth history, and its signature preserved despite ~4.45 Gyr of convection (Mukhopadhyay, 2012). The low I/Xe may have come from inefficient degassing of the deeper parts of the magma ocean, or low iodine abundances in the early-accreted materials.

The paired I-Pu-Xe decay system provides additional insight into early magma ocean history. Initially, catastrophic outgassing would have transported Xe out of the terrestrial magma ocean; after closure, products of ^{129}I decay and ^{244}Pu fission would have been retained in the silicate Earth. Because ^{129}I and ^{244}Pu decay at different rates, the $^{129}Xe^*/^{136}Xe_{Pu}$ ratio (where the star indicates radiogenic ^{129}Xe from the decay of ^{129}I, and the subscript denotes ^{136}Xe from Pu-fission; Mukhopadhyay, 2012) can be used to calculate a "closure age" that marks the end of open system magma ocean outgassing (Wetherill, 1975). The Iceland and Samoan Rochambeau Rift samples exhibit low $^{129}Xe^*/^{136}Xe_{Pu}$ ratios compared to the MORB mantle. If the whole mantle had an initially homogeneous I/Pu ratio, then low $^{129}Xe^*/^{136}Xe_{Pu}$ ratios in OIBs would indicate a late closure age for the OIB mantle relative to the MORB mantle, because less of the shorter-lived ^{129}I would remain at the onset of Xe retention in the mantle. A more realistic scenario may be that the mantle had an initially heterogeneous I/Pu, and regions of low I/Pu reflected limited accretion of volatile-rich materials into the OIB mantle (Mukhopadhyay, 2012; Caracausi et al., 2016; Parai et al., 2019). A relatively dry OIB mantle may have contributed to inefficient mixing in both the terrestrial magma ocean and the solid mantle over Earth history (Parai, 2022). Thus, the OIB I-Pu-Xe signature not only records heterogeneity in the early mantle, but also provides insight into the mechanisms that preserve heterogeneities formed during the early magma ocean.

The Effect of the Core on the OIB Source

Early core formation and its subsequent evolution likely play an important role controlling radiogenic and stable isotope variations in OIBs. The Earth's metallic core physically separated from the mantle during the first few tens of million years of Earth history (Kleine et al., 2002, Yin et al., 2022; Walker, 2014), and probably trapped a significant proportion of the lighter elements (e.g., ~ 10% of Si, O, S, C, N, and H; McDonough, 2016; Badro et al., 2015). Incorporation of these light elements into the core may have changed the isotopic composition of the mantle on a bulk scale (Shahar et al., 2016), however such fractionation would not generate mantle heterogeneities if core formation occurred when the entire mantle and the entire core were in equilibrium. For example, whole mantle-core equilibrium (Shahar et al., 2011) has been proposed to explain the observation that the mantle is fractionated in silicon isotopes relative to chondrites (Georg et al., 2007; Hin et al., 2017). In contrast, evidence from diamond inclusions suggests that iron (Fe) isotopic heterogeneities exist in Earth's deep mantle. Cullinan-like, Large, Inclusion-Poor, Pure, Irregular, and Resorbed (CLIPPIR) diamonds from Letseng, Lesotho, which originate from depths of 360–750 km, exhibit heavy Fe isotopic signatures ($\delta^{56}Fe$ = 0.79–0.90‰) that lie outside the near-0‰ range of known mantle compositions or expected reaction products at depth (Smith et al., 2021). High pressure and temperature experiments suggest that core formation on its own cannot account for such a large shift in Fe isotopic ratios (Elardo et al.,

2019). Rather, these data provide evidence for the subduction of surface material characterized by light isotopic ratios into the lower mantle (Smith et al., 2021).

Owing to the lack of temporal control on stable isotope signatures, it is plausible that the Fe stable isotope fractionation observed in the mantle reflects the cumulative effects of several processes. These processes likely include both interactions between the core and the mantle as well as the subtle but systematic heterogeneity in the convecting mantle caused by billions of years of subduction. To identify and untangle all the possible fractionation mechanisms within the mantle, more experiments need to be conducted in relevant pressure, temperature, and compositional space.

Core-Mantle Interactions

Due to the extremely high temperatures at the CMB, mantle minerals in direct contact with the liquid core may be in chemical equilibrium with that liquid. As the core cools and the composition of the outer core changes because of ongoing crystallization of the inner core, some elements may be diffusing across the core-mantle boundary as they are exsolved from the liquid outer core. Thus, the composition of the core could be changing progressively, and mantle heterogeneity may be increasing in response to the evolving core (Tronnes et al., 2019). Experimental work by Hayden and Watson (2007) has shown that grain-boundary diffusion is an efficient pathway for core-mantle interaction. In their experiments, siderophile elements diffused through MgO at a rate high enough to transport those elements across geological length scales (tens of kilometers) over 4.5 Ga.

Geochemical signatures of several highly siderophile elements suggest that the lower mantle was "polluted" with core material prior to being entrained into mantle plumes. The resulting signatures include elevated Fe/Mn ratios, such as those in Hawaiian lavas (Humayun et al., 2004), and radiogenic Os isotope enrichments detected in several mantle plumes on the world (Brandon et al., 1998, 2003). Subsequent studies (e.g., Ravizza et al., 2001), however, raise questions on these results. Despite further investigations (Brandon et al., 2003; 2005; Ireland et al., 2011), no other isotopic signature indicative of element transport across the core-mantle boundary was identified until the development of high precision $\mu^{182}W$ measurements (Touboul et al., 2012a; 2012b; Trinquier et al., 2016). Small negative anomalies in $\mu^{182}W$ (-25 ppm) have been measured in OIBs (Fig. 5b; Mundl et al., 2017; Mundl-Petermeier et al., 2019; 2020; Peters et al., 2021). In mantle-derived samples, the $\mu^{182}W$ shifts over time, from positive values in Hadean-Archean samples (4.3 to 2.7 Ga) to negative values in modern samples. This observation suggests that the W signature in OIB may reflect a time-integrated core contribution of tungsten to the mantle. The mechanism of interaction between the outer liquid core and the mantle remains debated, but current work is focused on Si-Mg-Fe oxide exsolution (Rizo et al., 2019) and diffusive exchange across the CMB between foundered oxidized, oceanic crust and the outer core (Mundl-Petermeier et al., 2020; Yoshino et al., 2020).

Core-mantle interactions may also manifest in the I-Xe system. If iodine were more strongly siderophile than Xe at core formation pressures and temperatures (Armytage et al., 2013; Jackson et al., 2018), the core would have had elevated I/Xe and I/Pu compared to the mantle. In this case, the core would supply high $^{129}Xe/^{130}Xe$ and $^{129}Xe^*/^{136}Xe_{Pu}$ to the mantle. However, OIBs sample a reservoir with low $^{129}Xe/^{130}Xe$ and $^{129}Xe^*/^{136}Xe_{Pu}$ compared to the rest

of the mantle. The core may have instead acted as a sink for lower mantle iodine during accretion, with no subsequent transfer of radiogenic Xe back to the mantle over time (Jackson et al., 2018).

The core has been posited as a potential source of high $^{3}He/^{4}He$ in the OIB source (Porcelli and Halliday, 2001; Bouhifd et al., 2020; Roth et al., 2019; Olson and Sharp, 2022). Negative $\mu^{182}W$ anomalies are broadly associated with elevated $^{3}He/^{4}He$ (Mundl et al., 2017; Mundl-Petermeier et al., 2019; 2020; Peters et al., 2021; Jackson et al., 2020a) in some lavas from Hawai'i, Samoa, Iceland, and the Galápagos, suggesting that core contributions could supply both negative $\mu^{182}W$ and high $^{3}He/^{4}He$ to material in the lower mantle. In detail, however, the highest OIB $^{3}He/^{4}He$ ratios are associated with modest negative $\mu^{182}W$, and the strongest negative $\mu^{182}W$ anomalies are associated with only moderate $^{3}He/^{4}He$.

Jackson et al. (2020a) suggested that recycled crust can mask He and W isotopic signatures, proposing that He and W anomalies may only persist in mantle domains that are the least affected by crustal recycling (consistent with the relationship between He isotopes and Th enrichment; Class and Goldstein, 2005). Nevertheless, the most negative $\mu^{182}W$ anomalies found to date are accompanied by strong indications of recycling in Kr and Xe isotopic compositions at Fernandina Island, Galápagos (Péron et al., 2021). There is likewise a pronounced recycling signature in the Kr and Xe isotopes at Iceland (Mukhopadhyay, 2012; Péron et al., 2021), where some of the highest $^{3}He/^{4}He$ ratios have been detected. Additional measurements of W and noble gases from samples that have also been thoroughly characterized for radiogenic isotopic compositions are needed to resolve the relationship between core-hosted signatures and contributions recycled versus primitive mantle domains.

Constraints on Lower Mantle Seismic Structures

Variations in the ^{182}Hf-^{182}W, I-Pu-Xe, and ^{146}Sm-^{142}Nd isotopic systems in OIBs require that plumes sample early-formed reservoirs, likely from the deepest part of the mantle (Fig. 5). Even though few lavas have been measured for all of these isotopic systems, the existing data provide insight into the nature of early-formed mantle reservoirs. The ULVZs are speculated to be the source of the high $^{3}He/^{4}He$ and the most negative $\mu^{182}W$ in OIBs (e.g., Jackson et al., 2017; Mundl et al., 2017; Williams et al., 2019; Kim et al., 2019). If, core-mantle interaction supplies high $^{3}He/^{4}He$ and the most negative $\mu^{182}W$ signatures (Rizo et al., 2019; Mundl-Petermeier et al., 2020; Peters et al., 2021), then the ULVZs may have formed via interactions with the core. An alternative mechanism to explain variable $\mu^{182}W$ anomalies in OIB is early silicate differentiation that modified the Hf/W ratios of mantle reservoirs, which subsequently remained mostly isolated from the rest of the convecting mantle throughout Earth history (e.g., Touboul et al., 2012a; Brown et al., 2014; Puchtel et al., 2016).

The LLSVPs, described as thermochemical piles, may represent relics of magma ocean crystallization after the Moon-forming giant impact (e.g., Labrosse et al., 2007; Lee et al., 2010 Ballmer et al., 2017; Gülcher et al., 2020). As noted above, variations in $\mu^{142}Nd$ measured in a few OIBs suggest that remnants of magma ocean crystallization may be preserved in the deep mantle (Peters et al., 2018). If the Moon-forming giant impact occurred ~4.4-4.35 Ga, as suggested by studies of both terrestrial and lunar samples (Morino et al., 2017; Borg et al., 2019; Lock et al., 2020), then the ^{182}Hf-^{182}W system was already extinct, which would leave the ^{182}W

isotope composition unchanged by the collision and explain the lack of correlation between $^{142}Nd/^{144}Nd$ and $^{182}W/^{184}W$ in OIB lavas (except for Réunion lavas; Peters et al., 2021). Alternatively, LLSVPs may have formed from the accumulation of subducted material (e.g., Brandenburg and van Keken, 2007; Nakagawa et al., 2009) or from the sinking of dense, reduced material (e.g., Gu et al., 2016; Creasy et al., 2020). Most likely, LLSVPs do not result from a single process, but incorporate material from primordial and early events, ongoing convection, and recycled subducted material (McNamara, 2019; Parai et al., 2019).

Section 6 Mantle Mixing and Convection

Linking the spatio-temporal geochemical variations of plume-derived lavas to the heterogeneous structure of the deep mantle requires an understanding of the internal dynamics of plumes which, in turn, depends on their rheology, composition, and excess temperature. In a purely thermal plume, assuming a Newtonian rheology, the morphology is controlled by the viscosity contrast between the hot plume and the colder ambient mantle. If the viscosity is strongly temperature-dependent, the plume develops a mushroom-shape, with a large head and a narrow tail (Richards et al., 1989). For a constant viscosity, the plume shape is finger-like (e.g., Whitehead and Luther, 1975; Korenaga, 2005). Moreover, the internal flow across a purely thermal plume depends on the viscosity contrast between the hot axial part of the conduit and its colder periphery; the vertical velocity is maximum at the plume axis and decreases exponentially with the square of the radial distance (e.g., Olson et al. 1993). Such a velocity profile generates zones with high strain rates, where passive geochemical heterogeneities get stretched into filaments (Kerr and Mériaux, 2004, Farnetani and Hofmann, 2009).

The lower mantle, however, is likely to be compositionally heterogeneous, which raises the question of how heterogeneous material entrained by a plume is deformed during upwelling and how the plume morphology and flow across the conduit are modified by those heterogeneities. Both laboratory experiments (e.g., Davaille 1999, Kumagai et al., 2008, Limare et al., 2019) and numerical simulations (e.g., Christensen and Hofmann, 1994, Tackley, 1998, Nakagawa and Tackley, 2014, Li et al., 2014, Gülcher et al., 2020, Jones et al., 2021) have explored global convection and plume dynamics in a heterogeneous mantle. Compositional heterogeneities are often simulated as intrinsically denser material (Gu et al., 2016), representing either eclogitic recycled crust, which is denser than the surrounding pyrolitic mantle (e.g., Hirose et al. 1999), or Fe-enriched, relatively primordial material (e.g., Deschamps et al., 2012, Nakagawa and Tackley, 2014, Li et al., 2014). Rheological heterogeneities are often simulated as more viscous domains (e.g., Ballmer et al., 2017; Gülcher et al., 2020), either because of a silica enrichment (e.g., Yamazaki et al., 2000, Ballmer et al., 2017), an increase in the mineral grain size (Ammann et al., 2010), and/or a reduction of the water content (Hirth and Kohlstedt, 1996; Karato, 2010; Parai, 2022). These studies indicate that variations in density and/or rheology profoundly affect convective mixing efficiency by promoting the long-term preservation of deep-seated heterogeneities.

Gülcher et al. (2021, Fig. 6) illustrates the results of numerical simulations of mantle plumes, featuring distinct lithological components: dense recycled basalt and the complementary depleted harzburgitic residue, a rheologically distinct bridgmanitic primordial material, and an ancient FeO-rich basal layer with the same physical properties as basalt. After 4.5 Ga of convection, part of the recycled oceanic crust accumulates at depth and forms large piles, while

the remainder is dispersed in the mantle, forming small streaks. The primordial material, intrinsically more viscous, partially survives as distinct "blobs", whereas a fraction of the ancient FeO-rich basal layer can be preserved by being incorporated into the denser basal piles. Numerical simulations (Farnetani et al., 2018) focusing on mantle plumes carrying finite size (30-40 km radius) rheological heterogeneities also indicate that intrinsically more viscous heterogeneities can resist stretching because they rotate during their ascent.

For thermo-chemical plumes, the subtle balance between positive thermal buoyancy and negative compositional buoyancy induces oscillatory behavior (Davaille, 1999) and complex internal dynamics, because some parts of the conduit may sink while others ascend (Kumagai et al., 2008). Furthermore, the idea that isotopic zonation in the plume conduit preserves the large-scale zonation in the mantle source region may not be accurate for thermo-chemical plumes because, under certain conditions, compositionally denser material rises preferentially at the plume axis (Jones et al., 2016). However, if chemical heterogeneity is a passive component of lower mantle structures (i.e., it has less effect on physical parameters such as density), and if lower mantle structures differ mainly in their thermal properties, then isotopic zonation could potentially be preserved in the plume conduit (Jones et al., 2016). Numerical simulations of mantle plumes carrying finite size (30-40 km radius) rheological heterogeneities, 20-30 times more viscous than the surrounding rocks, indicate that those heterogeneities do not stretch, but instead simply rotate as they ascend (Farnetani et al., 2018). Viscous material that resists stretching is more likely to preserve a distinct isotopic fingerprint.

Section 7 A New Paradigm for Mantle Plumes

The Hawaiian-Emperor chain has been used as the basis for many current paradigms related to mantle plumes (Morgan, 1971). Data accumulated from ocean islands worldwide, however, suggest that Hawai‘i may be the exception for plume behavior, rather than the type-model. For example, the Hawaiian system has the highest buoyancy flux and mantle potential temperature of any terrestrial plume (Fig. 1a; King and Adam, 2014; Putirka, 2008; Garcia et al., 2020), and younger segments of the Hawaiian chain record much higher melt flux than most other plumes (e.g., Putirka, 2008; Garcia et al., 2015; Wessel, 2016). Furthermore, the correlation between buoyancy flux, mantle potential temperature, and elevated $^{3}He/^{4}He$ supports the inference that the Hawaiian plume results from dynamical processes rooted in the deep mantle (Bao et al., 2022). Thus, the extent to which the Hawaiian plume can serve as the mantle plume archetype should be questioned; its importance as an accessible and well-studied but extreme example of intraplate volcanism, however, cannot be minimized.

Instead, OIBs may be evaluated more effectively using a range of variables, such as plume strength and temperature, source mantle composition, and melting conditions. We propose a mantle plume spectrum, based primarily on magma flux (King and Adam, 2014). The Hawaiian-Emperor chain defines the mantle plume end-member with the strongest magma production. Samoa, Iceland, and Galápagos are also classified close to the high-production end of the spectrum; all have in common high $^{3}He/^{4}He$ ratios in some of their erupted lavas, elevated buoyancy fluxes (Jackson et al., 2017), and the presence of slow velocity zones and an LLSVP at their source (e.g., Williams et al., 2019). The other end of the spectrum is represented by weaker plumes, with potentially shallower sources, which do not exhibit multiple mantle geochemical components nor have mantle potential temperatures significantly hotter than MORBs. Examples

at this end of the spectrum include Ascension, Juan de Fuca/Cobb-Eickelberg, and Bowie-Kodiak/Pratt-Welker, which have not been associated with a lower mantle seismic wave tomography anomaly that extends to the core-mantle boundary (i.e., French and Romanowicz, 2015), have isotopic compositions nearly indistinguishable from MORB (in part due to plume-ridge interaction, e.g., Bowie-Kodiak and Cobb-Eickelberg; Hegner and Tatsumoto, 1989; Chadwick et al., 2014), and are among the coolest mantle plumes (Bao et al., 2022).

Between the strong Hawaiian-type plumes and the weak Ascension-type systems are those that most closely emulate the classic model, such as Louisville, Kerguelen, Caroline, Easter, Réunion, and Tristan. These plumes possess a voluminous head that formed a LIP, followed by a plume tail and an age-progressive volcanic chain, and a buoyancy flux between ~0.5-2 Mg s^{-1} that wanes over time. The plume spectrum provides a reference framework for the comparison of mantle plumes and plume chemistry, which will prevent inappropriate comparisons between vastly dissimilar systems.

Section 8 Summary and Future Directions

Over the past couple of decades, the study of mantle plumes, their sources, and chemical heterogeneity in the mantle has generated important hypotheses and ideas about many of Earth's major processes, including convection, recycling, mantle residence times, and the nature of interactions between various reservoirs throughout the Earth system. It is no coincidence that advances in analytical geochemistry capabilities have paralleled the increasing sophistication of mantle plume models. The improvement in precision, sensitivity, and resolving power of mass spectrometers has opened new areas of the Periodic Table for analysis, including small isotopic anomalies, short-lived isotopic systems, and small mass-dependent fractionations that reflect early differentiation processes, recycling of subducted material into the mantle, and evidence for material preserved from Earth's earliest history.

The focused development of novel geochemical systems provides insight into large-scale planetary processes and compositional evolution, offering a rich area for future discoveries. Specifically, systems such as I-Pu-Xe, $^{182}W/^{184}W$, and $^{142}Nd/^{144}Nd$ have the potential to resolve interactions between the core and mantle, as well as examine the preservation and sampling of early-formed reservoirs in the mantle. The capabilities required to analyze rare noble gases and low-abundance W and Nd isotopes, however, exist in separate laboratories, necessitating collaborative efforts to generate insight from different isotopic systems on the same set of samples.

The improvement of analytical precision for the more commonly analyzed isotopic systems (e.g., Nd, Pb, and Hf isotopes) is essential to continue advancing the characterization of geochemical components in OIBs and examining differentiation processes throughout mantle history. This objective includes targeting melt inclusions, where extreme compositions from melted mantle heterogeneities may be captured prior to melt homogenization. Future work should also focus on exploring correlations across elemental and isotopic data sets. A database of high temperature and pressure isotopic fractionation factors will be essential to understand the processes affecting different isotopic systems.

Some of the greatest insights in mantle geochemistry have come from targeted sampling strategies, in which novel isotopic systems are applied to locations most likely to carry imprints of specific processes. Such studies require effective collaborations among laboratories and researchers, both for access to the advanced analytical techniques and to avoid analyzing sample powders separated from their geologic contexts.

Collaborative studies between geophysicists, geochemists, and geodynamicists are key to resolving important questions about how the transport of heterogeneities from Earth's mantle reservoirs to the surface is controlled by partial melting, plume-lithosphere, and plume buoyancy forces. Debate persists regarding how, during mantle transport, geochemical components are entrained, mixed, stretched, stalled, melted, and ultimately expressed in erupted lavas. This uncertainty propagates into the models that explain geochemical variations in erupted lavas, which rely on the interpretation of spatial patterns and time-integrated signatures in those lavas. A better understanding of mantle geodynamics, along with how lithology affects the melting and mixing of magmas, is needed to provide better constraints for understanding the source, evolution, and preservation of geochemical heterogeneities.

Finally, much is still unknown about the composition of seismically imaged mantle heterogeneities, in both the shallow and deep mantle and how they relate to chemical heterogeneities (e.g., Supplementary Fig. j, with a focus on the Pacific). The spatial differences in OIB compositions, both between different plume systems and over time at individual plumes, suggest systematic variations in mantle geochemical domains on many scales that are currently poorly understood. Resolving uncertainties in mantle geodynamics and melt homogenization processes will help determine whether these differences reflect distinct tectonic histories. Clearly, much remains to be learned about mantle plumes and the composition of the Earth; the greatest advances will likely emerge from cross-disciplinary studies in diverse fields such as experimental petrology, mineral physics, numerical geodynamics, seismology, and geochemistry.

Acknowledgements

DW acknowledges support from the Natural Sciences and Engineering Research Council of Canada through a Discovery Grant (From mantle geodynamics to environmental processes: a geochemical perspective) and from UBC for the Killam Professorship. KH received support from National Science Foundation grant RUI The Effect of a Mid-Ocean Ridge-Centered Environment on a Zoned Mantle Plume and Associated Secondary Magmatism (NSF award number 2018283). MB received funding from the European Research Council (ERC) under the European Union's Horizon 2020 research and innovation program (Grant Agreement No. 682778). CC acknowledges support from ERC (Grant Agreement No. 833632 – Survival of Hadean Remnants in a Dynamic mantle). RP was supported by NSF EAR 2145663.

Author contributions

The authors contributed to all aspects of the article. DW shared the vision and all authors contributed substantially to discussion of the content during various online meetings, as a group and for individual sections. All authors wrote the article. KH, LH, MB, and CC coordinated sections. LH and NW compiled data and helped for figures. All authors reviewed and/or edited the manuscript before submission.

Competing interests

The authors declare no competing interests.

Figures and captions

Figure 1a: Plume buoyancy flux by location (MilFil vol, Mg/s; King and Adam, 2014). The MilFil volume method calculates the mean depth anomaly within a 500 km diameter circle around a mantle plume, after filtering out small-scale features such as seamounts and islands. The MilFil volume is a proxy for the bathymetric swell generated by the underlying mantle plume, which is assumed to correlate with the magnitude of its flux. Circle diameters correspond to the magnitude of buoyancy flux. Colored circles: Plumes with geochemical data shown in figures 2-5. White circles: Mantle plume sites not included in subsequent geochemical figures in this review. Grey circles: Mantle plumes that lack flux estimates. Basemap: Tomography slice from the lowest mantle at 2800 km depth, extracted from the SEMUCB-WM1 model (French and Romanowicz, 2014), generated using the SubMachine online tool (Hosseini et al., 2018). Red regions define the seismically slow Pacific and African-Atlantic Large Low Shear Velocity Provinces (LLSVPs); blue regions are seismically faster parts of the lowermost mantle; velocity anomaly (dv/v) ranges from +2 to -2. Note the proximity of many mantle plumes relative to LLSVPs and how buoyancy flux of mantle plumes varies by orders of magnitude globally.

Figure 1b: Schematic cross-section of the mantle illustrating major mantle structures and locations of potential chemical reservoirs discussed in this review; the reservoirs are defined based on isotopic and trace element data from plume-generated OIB. Each reservoir is associated with a text box listing the isotopic systems that are especially useful for their identification and tracing (see text descriptions and Supplementary Table 2). Included are a heterogeneous LLSVP (indicated by different shades of orange, including mantle plumes), ULVZs (red), and subducted oceanic lithosphere (blue) that entrains recycled surface materials (e.g., sediments, indicated in brown). The plume, LLSVP, and ULVZ morphologies (whose thickness has been exaggerated so that it is visible at the scale of the diagram), are informed broadly by seismic studies (French & Romanowicz 2015; Wamba et al., 2023) and geodynamic results (Farnetani & Samuel, 2005; Davaille, 1999). The slab morphologies are guided roughly by seismic studies (Fukao & Obayashi, 2013; Garnero & McNamara, 2008) and geodynamic results (Jones at al., 2021; Nakagawa & Tackley, 2014). Of particular importance is the contribution of multiple mantle reservoirs, including recycled material, to the sources of mantle plumes.

Figure 2: Radiogenic isotope compositions of a selection of major ocean islands. (a) $^{206}Pb/^{204}Pb$ versus $^{208}Pb/^{204}Pb$; (b) $^{87}Sr/^{86}Sr$ versus $^{143}Nd/^{144}Nd$; (c) $^{143}Nd/^{144}Nd$ versus $^{176}Hf/^{177}Hf$; (d) $^{206}Pb/^{204}Pb$ versus $^{87}Sr/^{86}Sr$. Island chains are classified by their global end-members which are indicated by the colour of their field in the legend (as in Fig. 1a). In all panels, the grey field outlines Indian, Atlantic, and Pacific MORB. Labels indicate the location of end-member compositions: DMM is the depleted MORB mantle; EM-I is enriched mantle I; EM-II is enriched mantle II; HIMU is high μ (U/Pb); and PREMA is PREvalent MAntle. Data were downloaded from the GeoRoc geochemistry database in October 2021 (further details on the dataset and references are available in the supplementary information). Data density (panels

a-d) is contoured and indicates that most oceanic island basalts have contributions from PREMA plus at least one additional end-member.

Figure 3: Contributions of major mantle reservoirs to global plume buoyancy flux. Flux estimates (MiFil volumes; Mg/s) are from King and Adam (2014). Grey bars represent total buoyancy flux for each end-member, black lines are median values, and the distribution around the median for each mantle component is indicated by a coloured boxplot (color code as Fig. 1a). Plumes groups: **EM-I**: Meteor, Fernando de Noronha, Tasmantid, Lord Howe, Marion, Tristan da Cunha-Gough, Hawai'i-Emperor, Jan Mayen, Kerguelen, Pitcairn-Gambier, Rarotonga, Discovery-Shona. **EM-II**: St. Paul-Amsterdam, Azores, Marquesas, Samoa, Tahiti-Society. **PREMA**: Galápagos (also DM), Trindade-Martin, Crozet, Bouvet, Balleny, Ascension, Comores, Reunion, Bowie-Kodiak (or Pratt-Welker; currently erupting DM), Caroline, Easter-Salas y Gomez, Juan de Fuca (also known as Cobb-Eickelberg and Patton-Murray; currently erupting DM), Juan Fernandez, Louisville. **HIMU**: Vema, Bermuda, Cape Verde, Rurutu-Arago, St. Helena, Great Meteor, Canary, Macdonald (currently erupting PREMA), Baja-Guadalupe (also known as Fieberling), Socorro. **DM (depleted mantle, not depleted MORB mantle (DMM))**: Iceland, Madeira, San Felix. **Continental**: Yellowstone, East Africa, Eifel, Darfur, Afar (outlier in box plot), Tibesti, Cameroon, Hoggar, East Australia, Raton. EM-II and DM groups have highest median fluxes; EM-I has largest total flux, dominated by Hawai'i-Emperor; EM-I median flux is indistinguishable from PREMA and HIMU.
Mantle tetrahedron inset: Relationship between representative ocean island arrays and the five main mantle end-member compositions of Zindler and Hart (1986) in three-dimensional isotopic ratio space ($^{87}Sr/^{86}Sr$, $^{143}Nd/^{144}Nd$, $^{206}Pb/^{204}Pb$; Hart et al., 1992).

Figure 4: Lithium isotope compositions of ocean islands. (a) δ^7Li versus $^{206}Pb/^{204}Pb$; (b) Histogram of all current δ^7Li measurements on OIB. Separate island chains are indicated by the colour of their field in the legend, as in Fig. 1. In panel (a), the grey field includes data for Pacific, Atlantic, and Indian MORB. Labels indicate the location of end-member compositions, as in Fig. 2. OIB Lithium isotope data is from Chan et al., 2003; Kobayashi et al., 2004; Ryan and Kyle, 2004; Nishio et al., 2005; Chan et al., 2009; Vlastélic et al., 2009; Manga et al., 2011; Schusser et al., 2011; Krientiz et al., 2012, Genske et al., 2014; Harrison et al., 2015. MORB data in panel (a) is from Elliott et al., 2006, Tomascek et al., 2008, and Marschall et al., 2017. All Pb isotope values are normalized to the same standard values (SRM 981 value of 16.9405). Lithium isotopes trace fluid mobilization processes such as subduction (Bouman et al., 2004; Deschamps et al., 2010) and provide evidence for incorporation of recycled, subduction-altered material into the OIB source.

Figure 5: Use of isotopic systems to detect early Earth reservoirs. Only major ocean island systems discussed in this manuscript are shown. (a) $^{142}Nd/^{144}Nd$ in parts per million (ppm) deviation from the terrestrial standard (JNdi-1, AMES, or νNd-b). Baffin Island samples are included because they have the highest known $^3He/^4He$ ratios to date (up to 50 R_a; Stuart et al., 2003). Error bars: 2SE (Standard Error; sample measured once) or 2SD (Standard Deviation; samples measured several times), number of measurements indicated near symbol. External reproducibility (2SD) is estimated from repeated measurement of a standard reference material analyzed during the same analytical session as the samples, usually ~5 ppm (light grey, but Hyung and Jacobsen (2020) report a value of 1.1 ppm for 10 measurements of JNdi-1 (dark

grey)). Symbols outlined in red are those for which authors consider the deviation significant compared to external reproducibility (Réunion: Peters et al., 2018; Samoa: Horan et al., 2018). Data from: Andreasen et al., 2008; Murphy et al., 2010; Jackson and Carlson, 2012; Burkhardt et al., 2016; Saji et al., 2016; de Leeuw et al., 2017; Garçon et al., 2018; Horan et al., 2018; Peters et al., 2018; Hyung and Jacobsen, 2020. (b) $^{182}W/^{184}W$ measured in OIB samples (ppm deviation relative to terrestrial standard, *Alfa Aesar*). Error bars: 2SE or 2SD for samples. External reproducibility is ~ 4-5 ppm; large deficits measured in OIB samples can be resolved clearly. Samples from Baffin Island are not included because ^{182}W results are controversial. The positive $\mu^{182}W$ measured by Rizo et al. (2016) could be an analytical artifact (Kruijer and Kleine, 2018). Data from: Mundl et al., 2017; Mundl-Petermeier et al., 2019; Rizo et al., 2019; Peters et al., 2021. Small variations in extinct isotopic systems represent either potential contributions from early-formed material or core interaction with the plume source.
(c) $^{129}Xe/^{130}Xe$ in mantle sources for Iceland (Mukhopadhyay, 2012), Samoa (Rochambeau Rift; Peto et al., 2013) and Galápagos (accumulated gas; Péron et al., 2021). Error bars are 1SD following convention in the noble gas literature. The depleted mantle source is $^{129}Xe/^{130}Xe = 7.8$ from MORBs and well gases (Moreira et al., 1998; Holland and Ballentine, 2006; Parai et al., 2012; Tucker et al., 2012); atmospheric $^{129}Xe/^{130}Xe = 6.496$ (Basford et al., 1973), lower than OIB and MORB mantle sources. Noble gas systematics highlight the compositional differences between the MORB and OIB mantle sources.
(d) Neither post-eruptive atmospheric contamination (illustrated by the arrays of step-crush data trending toward atmospheric values) nor incorporation of regassed atmospheric Xe into the mantle can explain the OIB data arrays in $^{129}Xe/^{130}Xe$-$^{3}He/^{130}Xe$ space. The low $^{129}Xe/^{130}Xe$ in OIB mantle sources are thus interpreted to reflect a lower I/Xe ratio during the lifetime of ^{129}I compared to the upper mantle (Moreira et al., 1998; Parai and Mukhopadhyay, 2021).

Figure 6: Mantle convection simulations in two-dimensional spherical annulus geometry (Gülcher et al., 2021**).** Colors indicate distinct compositions: Basalt (blue, see also the composition triangle) ; Harzburgite (beige); a bridgmanitic primordial material (dark red), rheologically more viscous (by a factor λ_{prim}), initially forming a layer of thickness D_{prim}. The model also features an ancient FeO-rich basal layer (magenta) with the same physical properties of basalt. The inset shows the age of material forming the basal piles. Models illustrate that the mantle is strongly heterogeneous after 4.5 Gyr of model time.

Supplementary information

The online version contains supplementary material available at:

Supplementary Tables

Supplementary Table 1: Geochemical characteristics of the major mantle end-members as defined by Zindler and Hart (1986), adjusted according to subsequent research as cited in the table.

Supplementary Table 2: Summary of isotopic systems typically used in mantle geochemistry. Systems are listed as either radiogenic or stable. Included are the measured ratios and commonly used notations as well as the sources or processes traced.

Data Compilation

Figures 2, and Supplementary figures were constructed from a combined dataset of precompiled files for oceanic island groups from GeoRoc and several curated datasets (e.g., Weis et al., 2020; Harpp and Weis, 2020; Harrison et al., 2020). New data downloaded from the GeoRoc geochemistry database was done in October 2021 and included data from Azores, Easter and Salas-y-Gomez Islands, Iceland, Kerguelen, and St Helena. GeoRoc data selection criteria started with geological setting (Ocean Island), selection of ocean island chain, type of material (whole rock), and type of rock (volcanic rock). This was combined with data downloaded from GeoRoc in July 2020 and 2021, some of which is presented in Harrison et al. (2020). This data included Samoa, Cook-Austral Islands, Pitcairn-Gambier, Easter, Galápagos, Society, and Mauritius (see their supplementary information for a full list of references). New Pitcairn and Society trace element concentration and isotope composition data from Cordier et al. (2021) was added to the GeoRoc compilation, along with data from the Galápagos from Harpp and Weis (2020). Hawaiian-Emperor data was taken from Weis et al. (2020). The total number of samples in the compiled dataset was 19,824. The format of each of these precompiled files was standardized and imported into R, a free open-source software for statistical computing for analysis and plotting. All datasets except those downloaded in October 2021 were renormalized to the same standard values to ensure comparability (i.e., Weis et al., 2020). For major element and isotope plots, no filters were used on the dataset to assess data quality, which varied between labs, instrumentation, methods, and detection limits over the past forty to fifty years (much of this metadata is not included in the GeoRoc database, or is inconsistently included and therefore difficult to apply across such a varied dataset). Most isotopic data is post-1990. For trace element plots, a filter of SiO_2 greater than 55 and total alkalis (Na_2O+K_2O) less than 8 was applied to remove highly silica-undersaturated samples or samples that were produced by anomalously low degrees of partial melting. This removes samples with heavily enriched incompatible trace element concentrations, which would skew the average results presented in the extended trace element spider diagram.

Supplementary Figures

Major and trace element plots for a selection of major oceanic islands. DMM is the depleted MORB mantle; EM-I is enriched mantle I; EM-II is enriched mantle II; HIMU is high μ (U/Pb); and PREMA is PREvalent MAntle.

Figure (a): Total alkalis (Na_2O+K_2O) versus SiO_2 for a selection of major oceanic islands. The dashed line is the tholeiitic-alkalic divide line from Macdonald and Katsura (1964). Because of the large number of samples included in the figure (N = 19,691), the data have been contoured, clearly indicating that the vast majority of oceanic islands are basalts. The distribution frequency of the Na_2O+K_2O and SiO_2 data are shown along each axis on the right and top of the graph.

Figure (b): Average primitive mantle-normalized extended trace element compositions for a selection of major ocean islands. Averages were calculated for each oceanic island after removing all samples with $SiO_2 > 55$ wt.% and total alkalis (Na_2O+K_2O) < 8 to ensure that samples with elevated trace element concentrations caused by extremely low degrees of melting were not included in this compilation of average oceanic island compositions. Average trace element concentrations are normalized to primitive mantle values from McDonough and Sun (1995). Note the logarithmic scale. Details regarding data sources are provided in the supplementary information.

Figure (c-e): Trace element ratio plots for a selection of major oceanic islands. Important trace element ratio plots are shown of all ocean island basalts together and separated into ocean island groups. Because of the large number of samples in the figure, the data have been contoured using a kernel density estimation, in the general plot and in the panels for each oceanic island group. The distribution frequency of the data is shown along each axis on the right and top of the graph of all ocean island data plot. The subscript "PM" indicates that each element concentration was normalized to the primitive mantle values of McDonough and Sun (1995).
(c) $(La/Sm)_{PM}$ versus Th/Ta (N = 3,021)
(d) Nb/U versus Ce/Pb (N = 3,205)
(e) $(La/Sm)_{PM}$ versus Zr/Nb (N = 4,172).
Data contours are representative of the specific mantle end-member for each plot and are coloured accordingly

Figure (f-i) Radiogenic isotope compositions of a selection of major oceanic islands. These figures are the same as Fig. 2 with panels for each oceanic island group and one plot of all ocean islands plotted together. Kernel density estimation contours are drawn as in the trace element ratio supplementary figures.

Figure (j): Tomographic vertical cross-sections Bering Sea/NNW Pacific to southernmost Pacific. (a) Tomographic vertical cross-section from the Bering Sea/NNW Pacific Ocean to southernmost Pacific/Antarctic Ocean. Cross section captures the Hawai‘i, Tahiti-Society, and Macdonald plumes, marked by magenta circles and labeled as (H), (T), and (M), respectively. Tomographic model from SEMUCB-WM1 (French and Romanowicz, 2014). After imagery rendered using the SubMachine online tool (Hosseini et al., 2018). Warm colors are velocity-slow regions, and blue velocity-fast of the shear velocity (Vs) variations in each model. (b) Global map view showing the location and extent of the tomographic cross-section slice (black line intersecting black, white, and green circles). Symbols and labels as in (a).

Text Box #1

Mantle Plume and Large Igneous Province Fundamentals

Geodynamic models and analog experiments indicate that when plumes begin to rise through the mantle, upwelling material takes the form of a mushroom, with a large, semicircular head trailed by a narrow tail (Richards et al., 1989; Farnetani et al., 2002; Kerr and Mériaux, 2004; Lin and van Keken, 2006). Initial melt production is high, owing to the large volume of the plume head. When the plume head melts, it produces Large Igneous Provinces (LIPs) on land (e.g., Deccan, Siberian Traps), below sea level (e.g., Shatsky, Ontong-Java, Manihiki oceanic plateaus), or both (Kerguelen). This initial phase can last from one to several million years and requires involvement of significant volumes of mantle (Figure T1a). The LIP phase of plume activity is followed by a major reduction in melt production, which produces oceanic island basalts (OIBs) sourced from the plume tail; this phase often lasts 10s of millions of years (White and McKenzie, 1989; Sleep, 1990; Campbell and Griffiths, 1990; White, 1993; Kumagai et al., 2008).

The sheer size of plume heads requires a large volume of material from the lower mantle. Indeed, mantle plumes are associated with low seismic velocities, reflecting the elevated temperature of ascending mantle material (Montelli et al., 2006; Putirka et al., 2007). Seismic studies of the

lower mantle (e.g., Dziewonski and Woodhouse, 1987; Garnero, 2000; Masters et al., 2000; Garnero et al., 2007) have induced a profound shift in mantle plume models, which have evolved from the classical mushroom-shaped, thermal model toward more complex thermo-chemical structures. The internal dynamics of thermo-chemical plumes reflect the interplay between positive (thermal) and negative (compositional) buoyancy forces. Most often, the symmetrical geometry is lost (e.g., Tackley, 1998; Davaille, 1999, Farnetani and Samuel, 2005), since some parts of the plume conduit sink (Kumagai et al., 2008) while others ascend slowly.

The geochemical signatures of LIP phases reflect the complex relationship between compositional heterogeneity and the internal structures of mantle plumes. Components sampled by LIP melts include the plume material itself, upper mantle, and even lithospheric material, a signal often more strongly observed in LIPs emplaced on continents than in submarine settings. Geochemical contributions to LIPs can be identified using alteration-resistant, so-called "immobile elements," which include Th, Ti, Yb, and Nb. During mantle melting, these elements behave similarly and predictably, making them useful both as proxies for common mechanisms that affect mantle-derived melts and for different mantle and/or crustal components (e.g., Pearce et al., 2021). For example, elevated Th/Nb ratios in LIP melts reflect increased crustal contamination (Figure T1b). The TiO_2/Yb ratio increases with greater depth of melt generation (more melting in the garnet region of the mantle, >80 km); this ratio also gets larger as extent of partial melting decreases, a signature frequently observed in the OIB (plume tail) phase, when considerably less melt is being generated than during the LIP stage.

Case Study: The Kerguelen LIP

The Kerguelen mantle plume produced a hybrid LIP, continental flood basalts in the early stages, an oceanic plateau (<85 Ma) and a plume trail (Frey et al., 2002). Kerguelen preserves signatures of multiple components whose origins span from the lower mantle to the crust, providing a valuable cross-section of the mantle reservoirs supplying the Kerguelen plume (Fig. T1b). Kerguelen melts plot dominantly within the oceanic field, overlapping other LIP fields and extending slightly into the transitional area between MORB-dominant and OIB-dominant LIP melts (Weis and Frey, 2002). A few older samples also overlap with the EM-OIB and lithospheric fields, the latter of which is interpreted as crustal contamination of LIP melts and commonly observed in continental settings (Pearce et al., 2021).

Figure T1a: Relative volumes of several Large Igneous Provinces (LIPs), shown as cross-sections of spheres scaled to estimates of the volume of partial melting (minimum and maximum diameters for 5 and 30% melting respectively) during their emplacement (modified from Coffin and Eldholm, 1994). NAIP = North Atlantic Igneous Province (continental), CRFB = Columbia River Flood Basalts (continental).

Figure T1b: Discrimination diagram for Large Igneous Provinces (modified from Pearce et al., 2021). Variations along the y-axis indicate level of crust contamination, while variations along the x-axis correspond to increasing depth of melting. SZLM = Subduction Zone-Lithospheric Mantle, EM = Enriched Mantle, OIB = Ocean Island Basalt, MORB = Mid-Ocean Ridge Basalt, and OPB = Ocean Plateau Basalt (equivalent to LIP). Red circles are Kerguelen samples (Doucet et al., 2005; Frey et al., 2002; Yang et al., 1998), with background fields also shown for Ontong-Java, Deccan, CRFB, and NAIP. Data sources same as in Pearce et al. (2021).

Text Box #2

What is an isotope? Radiogenic versus Stable, Time Integration, and the Noble Gases

Isotopes of a chemical element have the same number of protons in their nucleus but differ in their number of neutrons. Consequently, they have the same atomic number and occupy the same position on the Periodic Table but have different masses. Their relative abundances are measured by a mass spectrometer. Isotopes can be classified into broad categories on the basis of their stability (or lack thereof) and formation pathways.

Radiogenic Isotopes

A radioactive isotope has an unstable atomic nucleus that emits radiation and is spontaneously transformed into another isotope, the radiogenic product. The decay rate of a radioactive isotope is characterized by its half-life, which is the time for a given amount of the parent isotope to decay to half of its initial amount.

Time is the primary variable that generates the observed differences in radiogenic isotopic compositions in geologic settings. For example, geochronology uses two categories of radioactive isotopes—those with long half-lives (> 100 Myr) and those with a short half-lives (<100 Myr) relative to geological timescales. Isotopes with a long half-life (e.g., ^{87}Rb, ^{147}Sm) are still decaying today and produce variations in the abundances of daughter products (in this example, ^{87}Sr and ^{143}Nd, which are measured as ratios relative to a stable isotope of the same element, ^{87}Sr/^{86}Sr and ^{143}Nd/^{144}Nd) that take millions to billions of years to develop. These isotopic systems are used for geochronology and fingerprinting sources of materials. Conversely, radioactive isotopes with geologically short half-lives have now fully decayed and are extinct. Variations in the radiogenic isotope ratios produced by the decay of isotopes with short half-lives provide information about events that happened in the first few 100 million years, very early in Earth's history.

Neodymium provides a good example of the differences between short and long half-life isotope systems. Neodymium has two radiogenic isotopes (^{142}Nd and ^{143}Nd) produced by the decay of two radioactive isotopes of Sm (^{146}Sm and ^{147}Sm) with very different half-lives: 103 Myr and 106 Gyr. Therefore, the two isotopic systems display isotopic variations that reflect entirely different processes; the ^{146}Sm-^{142}Nd system tracks the presence of early Earth material and the ^{147}Sm-^{143}Nd system documents long-term source changes. Whereas the ^{147}Sm-^{143}Nd system has been analytically accessible since the 1980s, the variations in ^{142}Nd due to ^{146}Sm decay are so small that measuring ^{142}Nd/^{144}Nd is almost at the limit of the current analytical capabilities of modern mass spectrometers, and only achievable since 2000.

Contrary to trace elements (i.e., elements that constitute less than 0.1 wt% of a rock or magma), radiogenic isotopic compositions are not affected by the degree of partial melting or the crystallization history of a melt. Radiogenic isotopic ratios (e.g., ^{87}Sr/^{86}Sr, ^{143}Nd/^{144}Nd, ^{206}Pb/^{204}Pb, ^{4}He/^{3}He or ^{177}Hf/^{176}Hf) of a basalt are therefore representative of the composition of the material that melted to produce the basalt. Consequently, they provide time-integrated information about its origin. In contrast, variations of extinct radiogenic isotopic systems (e.g.,

$^{142}Nd/^{144}Nd$, $^{182}W/^{184}W$, $^{129}Xe/^{130}Xe$) indicate the presence of material that differentiated from the rest of the mantle during accretion.

Stable Isotopes

Stable isotopes are those whose nucleus is stable, resulting in isotopic abundances that are invariant in time. Some of these isotopes, especially the light elements (H, Li, O, C, and N), can be fractionated by physical, biological and sometimes chemical processes, and are used to trace fractionation processes rather than the long-term evolution of the source of lavas. Examples include atmospheric weathering (O), groundwater interaction (H, O, C), sediment recycling (Li, Tl), and redox-changes (Fe).

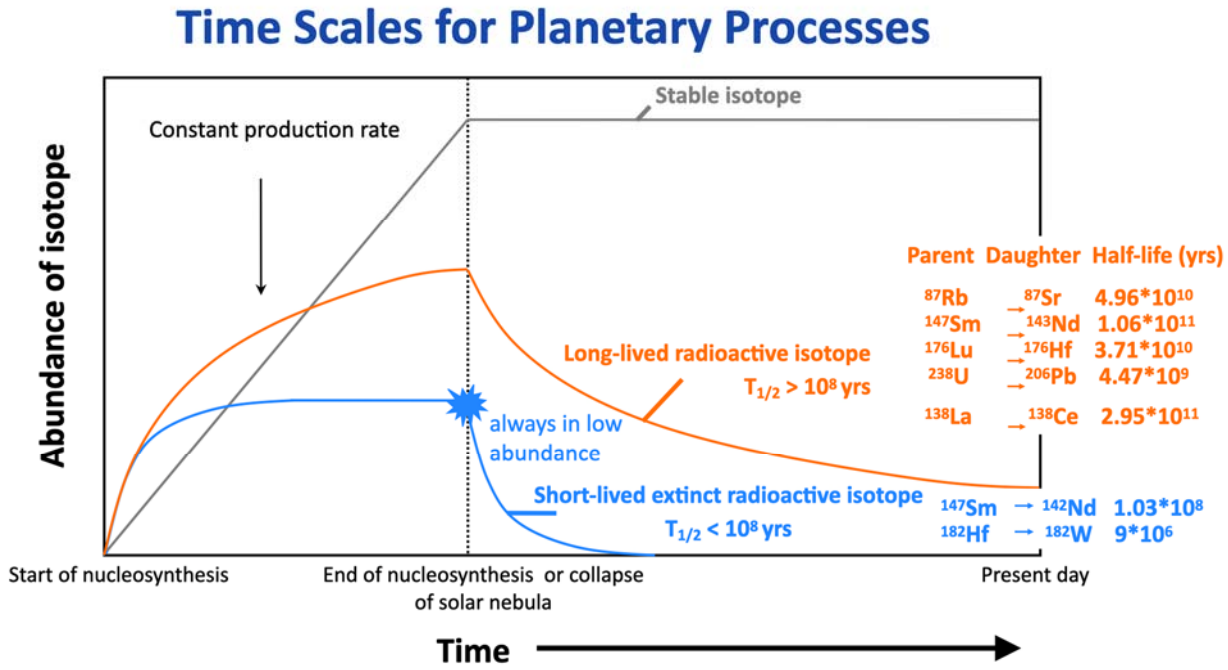

Noble Gases

All noble gases (sometimes called rare gases) have radiogenic and stable isotopes. For a wide variety of radioactive systems (Table 2), parent-daughter fractionation by gas loss within the lifetime of the radioactive isotope generates radiogenic noble gas isotope signatures over time.

The helium system provides a helpful example to illustrate important terms. In the helium system, ^3He is **primordial**, because it is a stable, non-radiogenic isotope whose abundance was established during accretion; any primordial isotopes lost to the atmosphere are not replaced in Earth's noble gas budget**.** Primordial noble gas isotopes are no different from the stable, non-radiogenic normalizing isotopes used in other decay systems (*e.g.*, ^{204}Pb). Accordingly, recent noble gas studies report He isotope ratios as $^4He/^3He$ to be consistent with radiogenic isotope convention. By contrast, ^4He is continuously produced by radioactive decay of ^{235}U, ^{238}U, and ^{232}Th (among other radioactive isotopes; ^4He is simply the alpha particle produced in these radioactive decay processes). Unradiogenic helium isotopic ratios reflect sampling of a reservoir that experienced less **degassing**, which is gas transport from the mantle to the atmosphere

associated with mantle processing by partial melting and volcanism. A **less-degassed** mantle reservoir has relatively high $^{3}He/^{4}He$ (and therefore lower $^{4}He/^{3}He$) because it has retained more of its primordial He, and the impact of radiogenic ingrowth of ^{4}He (through continuous alpha decay of radioactive U and Th) is muted compared to the rest of the mantle. A less-degassed reservoir is not necessarily primordial mantle. **Regassing** is the transport of atmospheric gases into the mantle via subducted slabs. Regassing of He is negligible as it is light enough to escape the atmosphere. Atmospheric contamination during or after sample formation affects Ne, Ar, Kr and Xe isotopic compositions measured in all OIBs. This impact can be corrected to determine the **mantle source** composition and assess whether regassing has affected the mantle.

Text Box #3
Analytical Precision in Determination of Radiogenic Isotopic Ratios

The measurement and the interpretation of isotopic variations measured in OIB require careful attention. For example, determinations of $^{142}Nd/^{144}Nd$ and $^{182}W/^{184}W$ ratios are mainly accomplished using thermal-ionization mass spectrometry (TIMS) techniques that allow high precision but also require considerable time and effort on the part of the analyst. Several studies indicate that analytical artifacts can produce small isotopic variations in TIMS measurements, which are linked to: 1) problematic mass-dependent fractionation correction when isotopic ratios do not follow the exponential law (Upadhyay et al., 2008); 2) inappropriate mass fractionation correction when the rate of mass fractionation is too high for dynamic measurements (Roth et al., 2014); 3) mixing of different sample reservoirs on the filaments (Upadhyay et al., 2008, Roth et al., 2014); 4) non-mass dependent isotopic variations (nuclear field shift) caused by the chemical separation protocol (Garçon et al., 2018; Kruijer and Kleine, 2018; Saji et al., 2016); and, just for the W system, 5) the need to improve the determination of O isotope composition for W isotope measurements done in oxide form by TIMS (Trinquier et al., 2016). Because deviations in the $^{142}Nd/^{144}Nd$ and $^{182}W/^{184}W$ systems are small, they are expressed in μ-notation (deviation in parts per million relative to the average ratio measured in the terrestrial standard).

High precision isotopic ratio measurements have revealed small differences between the terrestrial standards commonly used in the different laboratories (e.g., variation of a few parts per million in $^{142}Nd/^{144}Nd$ ratios measured in LaJolla, JNdi-1, and AMES Nd standard) that were likely produced during the purification process (O'Neil et al., 2008; Saji et al., 2016). The development of a method based on a multi-mass-step acquisition scheme allows for all isotopic ratios of the element to be determined in dynamic mode, with subsequent application of quality-control criteria (Garçon et al., 2018).

When publishing isotopic data, analytical uncertainty is reported as 2SD (standard deviation, calculated from repeated measurements of the same sample) or 2SE (standard error, where $2SE = 2SD/\sqrt{N}$, where N = number of measurements). The standard error corresponds to the internal error (based on counting statistics) when the sample is measured once. The scientific community has debated the significance of a deviation relative to its analytical precision extensively, without a clear resolution. Regardless of the choice of 2SD or 2SE, publications claiming high-precision isotopic measurements should thoroughly describe the analytical protocols used and all data associated with the measurement (interferences, mass bias, all measured ratios, and other phenomena that affect analytical results), as well as present the results for international, cross-

calibrated reference standard materials. Rigorous analysis also includes performing an appropriate number of duplicate, replicate, and total blank measurements.

A key factor in achieving high-precision isotopic measurements of oceanic island basalts is ensuring that only the original, magmatic composition of the basalt are measured, which is achieved primarily through appropriate sample preparation procedures. For example, Rb-Sr, U-Pb, and stable Li isotopic systems are susceptible to perturbation from seawater alteration, and Tl isotopic measurements are sensitive to the presence of ferromanganese precipitation. These secondary components must be removed by physical separation and cleaning followed by careful, systematic acid leaching procedures (Manhès et al., 1978; Dupré and Allègre, 1980; McDonough and Chauvel, 1991; Abouchami et al., 2000; Weis et al., 2006, 2007; Hanano et al., 2009; Nobre Silva et al., 2009, 2010; Williamson et al., 2021) to ensure that the measured data represent the original magmatic isotopic signatures representative of the magma source composition.

Finally, older OIB samples (> 7-10 Ma, depending on the isotopic system and analytical precision) must be age-corrected for in-situ decay since their eruption (e.g., Harrison et al., 2017; Harrison and Weis, 2018). This adjustment is especially important for samples where age correction will result in an isotopic ratio outside of the original analytical uncertainty, such as for Pb isotopic compositions in samples older than~15-20 Ma (Harrison et al., 2017). Age correction is completed using the decay equation and requires measurement of the elemental parent-daughter ratio of the unleached sample. For the U-Th-Pb system in particular, care must be taken to estimate the primary U concentration in submarine OIB properly, as U is susceptible to secondary alteration. For example, primary U can be estimated using the Th/U of unaltered samples (Nobre Silva et al., 2013b; Harrison et al., 2017).

Analytical Consistency and Comparability Between Labs

A particularly problematic challenge in OIB studies (and in any study where the objective is to determine the source compositions of rocks) involves comparison of data generated in different analytical laboratories on the same samples. To compare isotopic compositions generated using different instruments and methods (e.g., TIMS, MC-ICP-MS) and in different laboratories, geochemists use a normalization scheme based on published values for standards and reference materials (e.g., Weis et al., 2011, 2020). For robust comparisons, it is essential to perform careful normalization to the same standard and reference values. Otherwise, the data are not comparable and spurious correlations may occur.

References.

Abouchami, W., Galer, S. J. G. & Hofmann, A. W. High precision lead isotope systematics of lavas from the Hawaiian Scientific Drilling Project. *Chem. Geol.* **169**, 187–209 (2000).

Abouchami, W., Hofmann, A.W., Galer, S.J.G., Frey, F.A., Eisele, J. & Feigenson, M. Lead isotopes reveal bilateral asymmetry and vertical continuity in the Hawaiian mantle plume. *Nature* **434**, 851-856 (2005).

Allègre, C.J. Chemical geodynamics. *Tectonophysics* **81,** 109-132 (1982).

Ammann, M.W., Brodholt, J.P., Wookey, J. & Dobson, D.P. First-principles constraints on diffusion in lower-mantle minerals and a weak D" layer. *Nature* **465**, 462–465 https://doi .org /10 .1038 /nature09052 (2010).

Andreasen R., M. Sharma, K. V. Subbarao, S. G. Viladkar, Where on Earth is the enriched Hadean reservoir? *Earth Planet. Sci. Lett.***266**,14–28 (2008).

Armytage, R.M.G., Jephcoat, A.P., Bouhifd, M.A. & Porcelli, D. Metal-silicate partitioning of iodine at high pressures and temperatures: Implications for the Earth's core and (129)*Xe budgets. *Earth Planet. Sci. Lett.* **373**, 140-149 DOI10.1016/j.epsl.2013.04.031 (2013).

Avice, G. & Marty, B. Perspectives on atmospheric evolution from noble gas and nitrogen isotopes on Earth, Mars & Venus. *Space Sci Rev.* **216**, 1-18 (2020).

Badro, J., Brodholt, J.P., Pieta, H., Siebert, J. & Ryerso, F.J. Core formation and core composition from coupled geochemical and geophysical constraints. *Proc. Natl. Acad. Sci. USA* **112**, 12310–12314 (2015).

Ballmer, M.D., Houser, C., Hernlund, J.W., Wentzcovitch, R.M. & Hirose, K. Persistence of strong silica-enriched domains in the Earth's lower mantle. *Nat. Geosci.* **10**, 236–241. https://doi .org /10 .1038 /NGEO2898 (2017).

Bao, X., Lithgow-Bertelloni, C.R., Jackson, M.G. & Romanowicz, B. On the relative temperatures of Earth's volcanic hotspots and mid-ocean ridges. *Science* **375**, 57-61. DOI: 10.1126/science.abj8944 (2022).

Basford, J.R., Dragon, J.C., Pepin, R.O., Coscio Jr., M.R., Murthy, V.R. Krypton and xenon in lunar fines. Proceedings of the Lunar Science Conference. *Geochim. Cosmochim. Acta* Suppl. 4, 1915–1955 (1973).

Bekaert, D.V., Broadley, M.W., Caracausi, A. & Marty, B. Novel insights into the degassing history of Earth's mantle from high precision noble gas analysis of magmatic gas. *Earth Planet. Sci. Lett.* **525**, 115766 DOI10.1016/j.epsl.2019.115766 (2019).

Bizimis, M., Sen, G., Salters, V.J.M. & Keshav, S. Hf-Nd-Sr isotope systematics of garnet pyroxenites from Salt Lake Crater, Oahu, Hawaii: evidence for a depleted component in Hawaiian volcanism. *Geochim. Cosmochim. Acta* **69** (10), 2629–2646 (2005).

Blichert-Toft, J., Frey, F.A. & Albarède, F. Hf isotope evidence for pelagic sediments in the source of Hawaiian basalts. *Science* **285**, 879-882 (1999).

Blusztajn J., Nielsen S. G., Marschall H. R., Shu Y., Ostrander C. M. & Hanyu T. Thallium isotope systematics in volcanic rocks from St Helena - constraints on the origin of the HIMU reservoir. *Chem. Geol.* **476**, 292–301. doi:10.1016/j.chemgeo.2017.11.025 (2018).

Borg, L. E. et al. Isotopic evidence for a young lunar magma ocean. *Earth Planet Sc Lett* **523**, 115706 (2019).

Boschi, L., Becker, T.W. & Steinberger, S. Mantle plumes: Dynamic models and seismic images. *Geochem. Geophys. Geosyst.* **8(10)**, Q10006 (2007).

Bouhifd, M.A., Jephcoat, A.P., Porcelli, D., Kelley, S.P. & Marty, B. Potential of Earth's core as a reservoir for noble gases: Case for helium and neon. *Geochem. Perspect. Lett.* **15**, 15-18 DOI10.7185/geochemlet.2028 (2020).

Bouman, C., Elliott, T. & Vroon, P.Z. Lithium inputs to subduction zones. *Chem. Geol.* **212**, 59-79 (2004).

Boyet, M. & Carlson, R. W. 142Nd evidence for early (> 4.53 Ga) global differentiation of the silicate Earth. Science 309, 576–581 (2005).

Boyet, M., Doucelance, R., Israel, C., Bonnand, P., Auclair, D., Suchorski, K. & Bosq, C. New constraints on the origin of the EM-1 component revealed by the measurement of the La-Ce isotope systematics in Gough Island lavas. *Geochem. Geophys. Geosystems* **20**(5), 2484-2498 (2019).

Boyet, M., Garcon, M., Arndt, N., Carlson, R.W. & Konc, Z. Residual liquid from deep magma ocean crystallization in the source of komatiites from the ICDP drill core in the Barberton Greenstone Belt. *Geochim. Cosmochim. Acta* **304**, 141-159 DOI10.1016/j.gca.2021.04.020 (2021).

Brandenburg, J.P. & van Keken, P.E. Deep storage of oceanic crust in a vigorously convecting mantle. *J. Geophys. Res. Solid Earth* **112(B6),** B06403 DOI10.1029/2006JB004813 (2007).

Brandenburg, J.P., Hauri, E.H., van Keken, P.E. & Ballentine,C.J. A multiple-system study of the geochemical evolution of the mantle with force-balanced plates and thermochemical effects. *Earth Planet. Sci. Lett.* **276**, 1-13 (2008).

Brandon, A.D., Walker, R.J., Morgan, J.W., Norman, M.D. & Prichard, H.M. Coupled 186Os and 187Os evidence for core-mantle interaction. *Science* **280**, 1570–1573 (1998)

Brandon, A.D., Walker, R.J., Puchtel, I.S., Becker, H., Humayun, M. & Revillon, S. Os-186-Os-187 systematics of Gorgona Island komatiites: implications for early growth of the inner core. *Earth Planet. Sci. Lett.* **206**, 411-426 DOI10.1016/S0012-821X(02)01101-9 (2003).

Brandon, A.D., Humayun, M., Puchtel, I.S., Leya, I. & Zolensky, M. Osmium isotope evidence for an s-process carrier in primitive chondrites. *Science* **309**, 1233-1236 DOI10.1126/science.1115053 (2005).

Brett, A., Prytulak, J., Rehkämper, M., Hammond, S.J., Chauvel, C., Stracke, A. & Willbold, M. Thallium elemental and isotopic systematics in ocean island lavas. *Geochim. Cosmochim. Acta* **301**, 187-210 (2021).

Brown, S. M., Tanton, L. T. E. & Walker, R. J. Effects of magma ocean crystallization and overturn on the development of 142Nd and 182W isotopic heterogeneities in the primordial mantle. *Earth Planet. Sci. Lett.* **408**, 319–330 (2014).

Burkhardt, C., Borg, L.E., Brennecka, G.A., Shollenberger, Q.R., Dauphas, N., Kleine, T., 2016. A nucleosynthetic origin for the Earth's anomalous ^{142}Nd composition. *Nature* 537, 394–398 (2016).

Burke, K. & Torsvik, T. H. Derivation of Large Igneous Provinces of the past 200 million years from long-term heterogeneities in the deep mantle. *Earth Planet. Sci. Lett.* **227**, 531-538 (2004).

Burke, K., Steinberger, B., Torsvik, T.H. & Smethurst, M.A. Plume generation zones at the margins of large low shear velocity provinces on the core mantle boundary. *Earth Planet. Sci. Lett.* **265**, 49-60 (2008).

1427 Cabral, R.A., Jackson, M.G., Rose-Koga, E.F., Koga, K.T. Koga, Whitehouse, M.J. et al.
1428 Anomalous sulphur isotopes in plume lavas reveal deep mantle storage of Archaean crust.
1429 *Nature* **496(7446)** 490-493 (2013).
1430 Caffee, M.W., Hudson, G.B., Velsko, C., Huss, G.R., Alexander, Jr. E.C. & Chivas, A.R.
1431 Primordial noble gases from Earth's mantle: Identification of a primitive volatile
1432 component. *Science* **285**, 2115-2118 (1999).
1433 Campbell, I.H. & Griffiths, R.W. Implications of mantle plume structure for the evolution of
1434 flood basalts. *Earth Planet. Sci. Lett.* **99**, 79-93 (1990).
1435 Caracausi, A., Avice, G., Burnard, P.G., Furi, E. & Marty, B. Chondritic xenon in the Earth's
1436 mantle. *Nature* **533,** 82-85 DOI10.1038/nature17434 (2016).
1437 Castillo, P.R. The recycling of marine carbonates and sources of HIMU and FOZO ocean island
1438 basalts. *Lithos* **216–217**, 254-263 (2015).
1439 Chadwick, J., Keller, R., Kamenov, G., Yogodzinski, G. & Lupton, J. The Cobb hot spot:
1440 HIMU-DMM mixing and melting controlled by a progressively thinning lithospheric lid.
1441 *Geochem. Geophys. Geosystems* **15**, 3107–3122 (2014).
1442 Chan, L.-H. & Frey, F.A. Lithium isotope geochemistry of the Hawaiian plume: Results from the
1443 Hawaii Scientific Drilling Project and Koolau Volcano. *Geochem. Geophys. Geosystems*
1444 **4(3)**, 8707 (2003).
1445 Chan, L., Lassiter, J.C., Hauri, E.H., Hart, S.R. & Blusztajn, J. Lithium isotope systematics of
1446 lavas from the Cook-Austral Islands: Constraints on the origin of HIMU mantle. *Earth*
1447 *Planet. Sci. Lett.* **277**, 433-442 (2009).
1448 Chauvel, C., Hofmann, A.W. & Vidal, P. HIMU - EM - the French-Polynesian connection. *Earth*
1449 *Planet. Sci. Lett.* **110**, 99–119 (1992).
1450 Chauvel, C., McDonough, W., Guille, G., Maury, R. & Duncan, R. Contrasting old and young
1451 volcanism in Rurutu Island, Austral chain. *Chem. Geol.* **139,** 125-143 (1997).
1452 Chauvel, C., Lewin, E., Carpentier, M., Arndt, N.T. & Marini, J.-C. Role of recycled oceanic
1453 basalt and sediment in generating the Hf-Nd mantle array. *Nature Geosci.* **1(1)**: 64-67
1454 (2008).
1455 Chauvel, C., Maury, R.C., Blais, S., Lewin, E., Guillou, H., Guille, G., Rossi, P. & Gutscher, M.-
1456 A. The size of plume heterogeneities constrained by Marquesas isotopic stripes. *Geochem.*
1457 *Geophys. Geosystems* **13(1)**, Q07005 doi:10.1029/2012GC004123 (2012).
1458 Christensen, U. R. & Hofmann, A. W. Segregation of subducted oceanic crust in the convecting
1459 mantle, *J. Geophys. Res. Solid Earth* **99**, 19867-19884 (1994).
1460 Class, C. & Goldstein, S.L. Evolution of helium isotopes in the Earth's mantle. *Nature* **436**,
1461 1107-1112 DOI10.1038/nature03930 (2005).
1462 Coffin, M. & Eldholm, O. Large igneous provinces: crustal structure, dimensions, and external
1463 consequences. *Rev. Geophys.* **32**, 1–36 (1994).
1464 Cordier, C., Delavault, H. & Chauvel, C. Geochemistry of the Society and Pitcairn-Gambier
1465 mantle plumes: What they share and do not share. *Geochim. Cosmochim. Acta* **306** 362-
1466 384 (2021).
1467 Cottaar, S. & Romanowicz, B. An unsually large ULVZ at the base of the mantle near Hawaii.
1468 *Earth Planet. Sci. Lett*. **355**, 213–222 (2012).
1469 Cottaar, S., Martin, C., Li, Z. & Parai, R. The root to the Galápagos mantle plume on the core-
1470 mantle boundary. *Seismica* **1**, (2022).
1471 Courtillot, V., Davaille, A., Besse, J. & Stock, J. Three distinct types of hotspots in the Earth's
1472 mantle. *Earth Planet. Sci. Lett.* **205**, 295-308 (2003).

1473 Creasy, N., Girard, J., Eckert, J.O. & Lee, K.K.M. The role of redox on Bridgmanite crystal
1474 chemistry and calcium speciation in the lower mantle. *J. Geophys. Res. Solid Earth*
1475 **125(10),** 2020JB020783 DOI10.1029/2020JB020783 (2020).
1476 Dannenberg, J. & Sobolev, S. V. Low-buoyancy thermochemical plumes resolve controversy of
1477 classical mantle plume concept. *Nat. Comm.* **6**, 6960 (2015).
1478 Dasgupta, R., Hirschmann, M. M., & Smith, N. D. Partial melting experiments of peridotite+
1479 CO2 at 3 GPa and genesis of alkalic ocean island basalts. *J. Petrol.* **48(11),** 2093-2124
1480 (2007).
1481 Davaille, A. Simultaneous generation of hotspots and superswells by convection in a
1482 heterogeneous planetary mantle. *Nature* **402**, 756–760 (1999).
1483 Davies, D.R. & Davies, J.J. Thermally-driven mantle plumes reconcile multiple hot-spot
1484 observations. *Earth Planet. Sci. Lett.* **278**, 50-54 (2009).
1485 DeFelice, C., Mallick, S., Saal, A.E. & Huang, S. An isotopically depleted lower mantle
1486 component is intrinsic to the Hawaiian mantle plume. *Nat. Geosci.* **12**, 487–492 (2019.
1487 Delavault, H., Chauvel, C., Thomassot, E., Devey, C.W. & Dazas, B. Sulfur and lead isotopic
1488 evidence of relic Archean sediments in the Pitcairn mantle plume. *Proc. Natl. Acad. Sci.*
1489 *U.S.A.* **113(46)**: 12952-12956 (2016).
1490 de Leeuw, G.A.M., Ellam, R.M., Stuart, F.M. & Carlson, R.W. Nd-142/Nd-144 inferences on
1491 the nature and origin of the source of high He-3/He-4 magmas. *Earth Planet. Sci. Lett.* **472**,
1492 62-68 DOI10.1016/j.epsl.2017.05.005 (2017).
1493 DePaolo, D.J. Crustal growth and mantle evolution: inferences from models of element transport
1494 and Nd and Sr isotopes. *Geochim. Cosmochim. Acta* **44**, 1185–1196 (1980).
1495 DePaolo D. J. and Weis D. Hotspot Volcanoes and Large Igneous Provinces, in Continental
1496 Scientific Drilling: A Decade of Progress, and Challenges for the Future, Editors: U.
1497 Harms, C. Koeberl & M.D. Zoback, Springer, p. 259-288 (2007).
1498 Deschamps, F., Guillot, S., Godard, M., Chauvel, C., Andreani, M. & Hattori, K. In situ
1499 characterization of serpentinites from forearc mantle wedges: Timing of serpentinization
1500 and behavior of fluid-mobile elements in subduction zones. *Chem. Geol.* **269**, 262-277
1501 (2010).
1502 Deschamps, F., Cobden, L. & Tackley,P.J. The primitive nature of large low shear-wave velocity
1503 provinces. *Earth Planet. Sci. Lett.* **349-350**, 198-208 (2012).
1504 Dobson, D.P. & Brodholt, J.P. Subducted banded iron formations as a source of ultralow-
1505 velocity zones at the core-mantle boundary. *Nature* **434**, 371–374 (2005).
1506 Dorfman, S. M., Meng, Y., Prakapenka, V. B., & Duffy, T. S. Effects of Fe-enrichment on the
1507 equation of state and stability of (Mg,Fe)SiO3 perovskite. *Earth Planet. Sci. Lett.* **361**,
1508 249–257. https://doi.org/10.1016/j.epsl.2012.10.03 (2013).
1509 Dottin III, J. W., Labidi, J., Jackson, M. G., Woodhead, J. & Farquhar, J. Isotopic evidence for
1510 multiple recycled sulfur reservoirs in the Mangaia mantle plume. *Geochem. Geophys.*
1511 *Geosystems* **21(10)**, e2020GC009081 (2020).
1512 Doubrovine P.V., Steinberger, B. & Torsvik, T.H. A failure to reject: Testing the correlation
1513 between large igneous provinces and deep mantle structures with EDF statistics. *Geochem.*
1514 *Geophys. Geosystems* **17**, 1130-1163 doi:10.1002/2015GC006044 (2016).
1515 Doucet, S., Scoates, J., Weis, D. & Giret, A. Constraining the components of the Kerguelen
1516 mantle plume: A Hf-Pb-Sr-Nd isotopic study of picrites and high-MgO basalts from the
1517 Kerguelen Archipelago. *Geochem. Geophys. Geosystems* **6**, Q04007 (2005).

1518 Duncan, R.A., McCulloch, M.T., Barsczus, H.G. & Nelson, D.R. Plume versus lithospheric
1519 sources for melts at Ua Pou, Marquesas Islands. *Nature* **322**, 534–538 (1986).
1520 Duvernay, T., Davies, D.R., Mathews, C.R., Gibson, A. H. & Kramer, S.C. Linking Intraplate
1521 Volcanism to Lithospheric Structure and Asthenospheric Flow. *Geochem Geophys*
1522 *Geosystems* **22**, *e2021GC009953* (2021).
1523 Dupré, B. & Allègre, C. J. Pb–Sr–Nd isotopic correlation and the chemistry of the North Atlantic
1524 mantle. *Nature* **286**, 17–22 (1980).
1525 Dziewonski, A.M. & Woodhouse, J.H. Global images of the Earth's interior. *Science* **236**, 37–48
1526 (1987).
1527 Elderfield, H. The oceanic chemistry of the rare-earth elements. *Philos. Trans. R. Soc. London.*
1528 *Series A* **325**(1583), 105-126 (1988).
1529 Eisele, J., Sharma, M., Galer, S.J.G., Blichert-Toft, J., Devey, C.W. & Hofmann, A.W. The role
1530 of sediment recycling in EM-1 inferred from Os, Pb, Hf, Nd, Sr isotope and trace element
1531 systematics of the Pitcairn hotspot. *Earth Planet. Sci. Lett.* **196**, 197-212 Doi:
1532 10.1016/S0012-821X(01)00601-X (2002).
1533 Elardo, S. M., Shahar, A., Mock, T. D. & Sio, C. K. The effect of core composition on iron
1534 isotope fractionation between planetary cores and mantles. *Earth Planet Sc Lett* **513**, 124–
1535 134 (2019).
1536 Elliott, T., Thomas, A., Jeffcoate, A. & Niu, Y. Lithium isotope evidence for subduction-
1537 enriched mantle in the source of mid-ocean-ridge basalts. *Nature*, **443**, 565-568 (2006).
1538 Farley K.A., Natland J.H. & Craig H. Binary mixing of enriched and undegassed (primitive?)
1539 mantle components (He, Sr, Nd, Pb) in Samoan lavas. *Earth Planet. Sci. Lett.* **111**, 183–
1540 199 (1992).
1541 Farnetani, C.G., Legras, B. & Tackley, P.J. Mixing and deformation in mantle plumes. *Earth*
1542 *Planet. Sci. Lett.* **196(1)** 1-15 (2002).
1543 Farnetani, C.G. & Samuel, H. Beyond the thermal plume paradigm. *Geophys. Res. Lett.* **32**,
1544 L07311 (2005).
1545 Farnetani, C.G. & Hofmann, A.W. Dynamics and internal structure of a lower mantle plume
1546 conduit. *Earth Planet. Sci. Lett.* **282**, 314-322 (2009).
1547 Farnetani, C.G., Hofmann, A.W. & Class, C. How double volcanic chains sample geochemical
1548 anomalies from the lowermost mantle. *Earth Planet. Sci. Lett.* **359–360**, 240–247 (2012).
1549 Farnetani, C.G., Hofmann, A.W., Duvernay T. & Limare A. Dynamics of rheological
1550 heterogeneities in mantle plumes. *Earth Planet. Sci. Lett.* **499**, 74–82 (2018).
1551 Farquhar, J., Peters, M., Johnston, D.T., Strauss, H., Masterson, A., Wiechert, U. & Kaufman,
1552 A.J. Isotopic evidence for Mesoarchaean anoxia and changing atmospheric sulphur
1553 chemistry. *Nature* **449(7163)** 706-709 (2007).
1554 Faure P., Boyet M., Bouhifd M.A., Manthilake G., Hammouda T. and Devidal J.-L..
1555 Determination of the refractory enrichment factor of the bulk silicate Earth from metal-
1556 silicate experiments on Rare Earth Elements. *Earth Planet. Sci. Lett.,* **554**, 116644 (2021).
1557 Fourel, L., Limare, A., Jaupart, C., Surducan, E., Farnetani, C.G., Kaminski, E.C., Neamtu, C. &
1558 Surducan, V. The Earth's mantle in a microwave oven: thermal convection driven by a
1559 heterogeneous distribution of heat sources, *Exp. Fluids*, 58:90 DOI 10.1007/s00348-017-
1560 2381-3 (2017).
1561 French, S.W. & Romanowicz, B. Whole-mantle radially anisotropic shear velocity structure from
1562 spectral-element waveform tomography. *Geophys. J. Int.* **199**, 1303–1327 (2014).

French, S.W. & Romanowicz, B. Broad plumes rooted at the base of the Earth's mantle beneath major hotspots. *Nature* **525**, 95-99 (2015).
Frey, F. A., Weis, D., Borisova, A. & Xu, G. Involvement of continental crust in the formation of the Cretaceous Kerguelen Plateau: New perspectives from ODP Leg 120 sites. *J. Petrol.* **43**, 1207–1239 (2002).
Frey, F.A., Huang, S., Blichert-Toft, J., Regelous, M. & Boyet, M. Origin of depleted components in basalt related to the Hawaiian hot spot: evidence from isotopic and incompatible element ratios. *Geochem. Geophys. Geosystems* **6**, Q02L07 (2005).
Frossard, P., Israel, C., Bouvier, A. & Boyet, M. Earth's composition was modified by collisional erosion. *Science* **377**, 1529–1532 (2022).
Fukao, Y. & Obayashi, M. Subducted slabs stagnant above, penetrating through, and trapped below the 660 km discontinuity, *J. Geophys. Res. Solid Earth* **118, 11**, 5920-5938 https://doi.org/10.1002/2013JB010466 (2013).
Gale, A., Dalton, C.A., Langmuir, C.H., Su, Y. & Schilling, J.G. The mean composition of ocean ridge basalts. *Geochem. Geophys. Geosystems* **14**, 489-518 (2013).
Garapić, G., Jackson, M.G., Hauri, E.H., Hart, S.R., Farley, K.A., Blusztajn, J.S. & Woodhead, J.D. A radiogenic isotopic (He-Sr-Nd-Pb-Os) study of lavas from the Pitcairn hotspot: Implications for the origin of EM-1 (enriched mantle 1). *Lithos* **228**, 1-11 DOI10.1016/j.lithos.2015.04.010 (2015).
Garcia MO., Smith JR., Tree JP., Weis D., Harrison L., Jicha BR. Petrology, geochemistry, and ages of lavas from Northwest Hawaiian Ridge volcanoes, in Neal, C.R., Sager, W.W., Sano, T., and Erba, E., eds., The Origin, Evolution, and Environmental Impact of Oceanic Large Igneous Provinces. *Spec. Pap. Geol. Soc. Am.* **511**, p. 1–25, doi: 10 .1130 /2015 .2511 (01) (2015).
Garcia, M. O., Tree, J. P., Wessel, P. & Smith, J. R. Pūhāhonu: Earth's biggest and hottest shield volcano. *Earth Planet. Sci. Lett.* **542**, 116296 (2020).
Garcon, M., Boyet, M., Carlson, R.W., Horan, M.F., Auclair, D. & Mock, T.D. Factors influencing the precision and accuracy of Nd isotope measurements by thermal ionization mass spectrometry. *Chem. Geol.* **476,** 493-514 DOI10.1016/j.chemgeo.2017.12.003 (2018).
Garnero, E.J. Heterogeneity of the lowermost mantle, *Ann. Rev. Earth Planet. Sci.* **28**, 509-537 (2000).
Garnero, E., Lay, T. & McNamara, A. Implications of lower mantle structural heterogeneity for existence and nature of whole mantle plumes. *Spec. Pap. Geol. Soc. Am.* **430**, Plates, Plumes, and Planetary Processes 79–101 (2007).
Garnero, E.J. & McNamara, A. Structure and dynamics of Earth's lower mantle. *Science* **320**, 626-628 (2008).
Garnero, E.J., McNamara, A.K. & Shim, S.H. Continent-sized anomalous zones with low seismic velocity at the base of the Earth's mantle. *Nat. Geosci.* **9**, 481-489 (2016).
Gast, P.W. Trace element fractionation and the origin of tholeiitic and alkaline magma types. *Geochim. Cosmochim. Acta* **32**: 1057-1086 (1968).
Georg, R.B., Reynolds, B.C., West, A.J., Burton, K.W. & Halliday, A.N. Silicon isotope variations accompanying basalt weathering in Iceland. *Earth Planet. Sci. Lett.* **261**, 476-490 DOI10.1016/j.epsl.2007.07.004 (2007).

1607 Genske, F.S., Turner, S.P., Beier, C., Chu, M.-F., Tonarini, S., Pearson, N.J. & Haas, K.M.
1608 Lithium and boron isotope systematics in lavas from the Azores islands reveal crustal
1609 assimilation. *Chem. Geol.* **373**, 27-36 (2014).
1610 Genske, F., Stracke, A., Berndt, J. & Klemme, S. Process-related isotope variability in oceanic
1611 basalts revealed by high-precision Sr isotope ratios in olivine-hosted melt inclusions.
1612 *Chem. Geol.* **524**, 1–10 (2019).
1613 Gonnermann, H.M., & Mukhopadhyay, S. Preserving noble gases in a convecting
1614 mantle. *Nature*, *459*(7246), 560-563 (2009).Graham, D. W. Noble gas isotope
1615 geochemistry of mid-ocean ridge and ocean island basalts: Characterization of mantle
1616 source reservoirs. *Rev. Mineral. Geochem.* **47(1)**, 247-317 (2002).
1617 Gu, T., Li, M., McCammon, C., Lee, K.K.M., Redox-induced lower mantle density contrast and
1618 effect on mantle structure and primitive oxygen. *Nature Geosci* .**9**, 723–727
1619 https://doi.org/10.1038/ngeo2772 (2016).
1620 Gülcher, A.J.P., Gebhardt, D.J., Ballmer, M.D. & Tackley, P.J. Variable dynamic styles of
1621 primordial heterogeneity preservation in the Earth's lower mantle, *Earth Planet. Sci. Lett.*
1622 **536**, 116160 (2020).
1623 Gülcher, A.J.P., Ballmer, M.D., & Tackley, P.J. Coupled dynamics and evolution of primordial
1624 and recycled heterogeneity in Earth's lower mantle. *Solid Earth* **12**, 2087–2107 (2021).
1625 Haase, K.M., Beier, C. & Kemner, F. A comparison of the magmatic evolution of Pacific
1626 intraplate volcanoes: constraints on melting in mantle plumes. *Front. Earth Sci.* **6**, 242 doi:
1627 10.3389/feart.2018.00242 (2019).
1628 Hanan, B.B. & Graham, D.W. Lead and helium isotope evidence from oceanic basalts for a
1629 common deep source of mantle plumes. *Science* **272** 991-995
1630 DOI10.1126/science.272.5264.991 (1996).
1631 Hanano, D., Scoates, J. S. & Weis, D. Alteration mineralogy and the effect of acid-leaching on
1632 the Pb-isotope systematics of ocean-island basalts. *Am. Min.* **94**, 17–26 (2009).
1633 Harpp, K.S. & White, W.M. Tracing a mantle plume: Isotopic and trace element variations of
1634 Galapagos seamounts. *Geochem. Geophys. Geosystems* **2** DOI10.1029/2000GC000137
1635 (2001).
1636 Harpp, K.S., Hall, P.S. & Jackson, M.G. Galápagos and Easter: A tale of two hotspots. In:
1637 Harpp, K.S., Mittelstaedt, E., d'Ozouville, Noémi, Graham, D.W. (Eds.), The Galápagos:
1638 A natural laboratory for the earth sciences. *Geophys. Monog. Series* **204**, American
1639 Geophysical Union, 27-40 (2014).
1640 Harpp, K.S. & Geist, D.J. The Evolution of Galapagos Volcanoes: An Alternative Perspective.
1641 *Frontiers in Earth Science* **6**, 50 DOI10.3389/feart.2018.00050 (2018).
1642 Harpp K. & Weis D. Insights into the origins and compositions of mantle plumes: A comparison
1643 of Galapagos and Hawai'i. *Geochem. Geophys. Geosystems* **21**, e2019GC008887.
1644 https://doi.org/10.1029/2019GC008887 (2020).
1645 Harrison, L.N., Weis, D., Hanano, D. & Barnes, E. Lithium isotopic signature of Hawaiian
1646 basalts. In: Carey, R., Cayol, V., Poland, P., Weis, D. (Eds.), Hawaiian volcanoes: From
1647 source to surface. *Geophys. Monog. Ser.* **208**, American Geophysical Union, 74-104
1648 (2015).
1649 Harrison, L., Weis, D. & Garcia, M.O. The link between Hawaiian mantle plume composition,
1650 magmatic flux, and deep mantle geodynamics. *Earth Planet. Sci. Lett.* **463**, 298-309,
1651 (2017).

Harrison, L.N. & Weis, D. The size and emergence of geochemical heterogeneities in the Hawaiian mantle plume constrained by Sr-Nd-Hf isotopic variation over ~47 million years. *Geochem. Geophys. Geosystems* **19** doi:10.1029/2017GC007389 (2018).

Harrison, L.N., Weis, D. & Garcia, M.O. The Multiple Depleted Mantle Components in the Hawaiian-Emperor Chain. *Chem. Geol.* **532**, DOI: 10.1016/j.chemgeo.2019.119324, 1-22 (2020).

Hart, S.R., Hauri, E. H., Oschmann, L. A. & Whitehead J. A. Mantle plumes and entrainment: isotopic evidence. *Science* **256**, 517–520 (1992).

Hayden, L.A. & Watson, E.B. A diffusion mechanism for core-mantle interaction. *Nature* **450**, 709-711 DOI10.1038/nature06380 (2007).

Hegner, E. & Tatsumoto, M. Pb, Sr, and Nd isotopes in seamount basalts from the Juan de Fuca Ridge and Kodiak-Bowie Seamount chain northeast Pacific. *J. Geophys. Res. Solid Earth* **94(B12)** 17839-17846 (1989).

Hernlund, J. W. & McNamara, A.K. The Core-Mantle boundary region. *Treatise on Geophysics,* 2nd edition, **7**, 461-519 (2015).

Hirose, K., Fei, Y., Ma, Y. & Mao, H-K. The fate of subducted basaltic crust in the Earth's lower mantle. *Nature* **397**, 53-56 (1999).

Hin, R.C., Coath, C.D., Carter, P.J., Nimmo, F., Lai, Y.-G., Pogge von Strandmann, P.A.E., Willbold, M., Leinhardt, Z.M., Walter, M.J., Elliott, T. Magnesium isotope evidence that accretional vapour loss shapes planetary compositions. *Nature* **549**, 511–515 (2017).

Hirth, G. & Kohlstedt, D.L. Water in the oceanic upper mantle: implications for rheology, melt extraction and the evolution of the lithosphere. *Earth Planet. Sci. Lett.* **144**, 93–108 (1996).

Hofmann, A.W. & White, W.M. Mantle plumes from ancient oceanic-crust. *Earth Planet. Sci. Lett.* **57**, 421–436 (1982).

Hofmann, A.W., Jochum, K., Seufert, M. & White, W.M. Nb and Pb in oceanic basalts - new constraints on mantle evolution. *Earth Planet. Sci. Lett.* **79**, 33–45 (1986).

Hofmann, A.W. Mantle geochemistry: the message from oceanic volcanism. *Nature* **385**, 219-229 (1997).

Hofmann, A.W. Sampling mantle heterogeneity through oceanic basalts: Isotopes and trace elements. In: Carlson, R. (Ed.), *Treatise on Geochemistry* (first ed.) **2**, 61-102 (2003).

Hofmann, A. W., Class, C. & Goldstein, S. L. Size and Composition of the MORB+OIB Mantle Reservoir. *Geochem. Geophys. Geosystems* **23**, e2022GC010339. https://doi.org/10.1029/2022GC010339 (2022).

Holland, G. & Ballentine, C. J. Seawater subduction controls the heavy noble gas composition of the mantle. *Nature* **441**, 186-191, doi:Doi 10.1038/Nature04761 (2006).

Homrighausen, S., Hoernle, K., Hauff, F., Geldmacher, J., Wartho, J. A., van den Bogaard, P. & Garbe-Schönberg, D. Global distribution of the HIMU end member: Formation through Archean plume-lid tectonics. *Earth-Science reviews* **182**, 85-101 (2018).

Horan, M., Carlson, R.W., Walker, R.J., Jackson, M., Garcon, M. & Norman, M. Tracking Hadean processes in modern basalts with 142-Neodymium. *Earth Planet. Sci. Lett.* **484**, 184–191 DOI10.1016/j.epsl.2017.12.017 (2018).

Hosseini, K., Matthews, K. J., Sigloch, K.,Shephard, G. E., Domeier, M., & Tsekhmistrenko, M. SubMachine: Web-based tools forexploring seismic tomography andother models of Earth's deep interior. *Geochem. Geophys. Geosystems* **19**, 1464–1483. https://doi.org/10.1029/2018GC007431 (2018).

1697 Hyung, E. & Jacobsen, S. B. The $^{142}Nd/^{144}Nd$ variations in mantle-derived rocks provide
1698 constraints on the stirring rate of the mantle from the Hadean to the present. *Proc. Natl.*
1699 *Acad. Sci. U.S.A.* **117**, 14738–14744 (2020).
1700 Huang, S., Hall, P.S. & Jackson, M.G. Geochemical zoning of volcanic chains associated with
1701 Pacific hotspots. *Nat. Geosci.* **4(12)**, 874-878 (2011).
1702 Humayun, M., Qui, L. & Norman, M.D. Geochemical evidence for excess iron in the mantle
1703 beneath Hawaii. *Science* **306**, 91-94 (2004).
1704 Humphris, S.E., Thompson, G., Schilling, J.-G. & Kingsley, R.H. Petrological and geochemical
1705 variations along the Mid-Atlantic Ridge between 46°S and 32°S: Influence of the Tristan
1706 da Cunha mantle plume. *Geochim. Cosmochim. Acta* **49**, 1445-1464 (1985).
1707 Hyung, E. & Jacobsen, S. B. The $^{142}Nd/^{144}Nd$ variations in mantle-derived rocks provide
1708 constraints on the stirring rate of the mantle from the Hadean to the present. *Proc. Natl.*
1709 *Acad. Sci. U.S.A.* **117**, 14738–14744 (2020).
1710 Ireland, T.J., Walker, R.J., & Brandon, A.D., ^{186}Os-^{187}Os systematics of Hawaiian picrites
1711 revisited: New insights into Os isotopic variations in ocean island basalts. *Geochim.*
1712 *Cosmochim. Acta* **75**, 4456-4475 (2011).
1713 Israel, C., Boyet, M., Doucelance, R., Bonnand, P., Frossard, P., Auclair, D. & Bouvier, A.
1714 Formation of the Ce-Nd mantle array: Crustal extraction vs. recycling by subduction.
1715 *Earth Planet. Sci. Lett.* ***530***, 115941 (2020).
1716 Ito, G., Lin, J. & Gable, C.W. Dynamics of mantle flow and melting at a ridge-centered hotspot:
1717 Iceland and the Mid-Atlantic Ridge. *Earth Planet. Sci. Lett.* **144** 53-74 DOI10.1016/0012-
1718 821X(96)00151-3 (1996).
1719 Jackson, M.G., Kurz, M.D., Hart, S.R. & Workman, R.K. New Samoan lavas from Ofu Island
1720 reveal a hemispherically heterogeneous high He-3/He-4 mantle. *Earth Planet. Sci. Lett.*
1721 **264**, 360-374 DOI10.1016/j.epsl.2007.09.023 (2007).
1722 Jackson, M.G. & Dasgupta, R. Compositions of HIMU, EM1, and EM2 from global trends
1723 between radiogenic isotopes and major elements in ocean island basalts. *Earth Planet. Sci.*
1724 *Lett.* **276,** 175-186 doi:10.1016/j.epsl.2008.09.023 (2008).
1725 Jackson, M.G., Weis, D. & Huang, S. Major element variations in Hawaiian shield lavas: Source
1726 features and perspectives from global ocean island basalt (OIB) systematics. *Geochem.*
1727 *Geophys. Geosystems* **13**, 919 Q09009, doi:10.1029/2012GC004268 (2012).
1728 Jackson, M.G. & Carlson, R.W. Homogeneous superchondritic 142Nd/144Nd in the mid-ocean
1729 ridge basalt and ocean island basalt mantle. *Geochem. Geophys. Geosystems* **13**,1–10
1730 (2012).
1731 Jackson, M.G., Hart, S.R., Konter, J.G., Kurz, M.D., Blusztajn, J. & Farley, K.A. Helium and
1732 lead isotopes reveal the geochemical geometry of the Samoan plume. *Nature* **514**, 355–358
1733 (2014).
1734 Jackson, M.G., Konter, J.G., Becker, T.W. Primordial helium entrained by the hottest mantle
1735 plumes. *Nature* **542**, 340-343 (2017).
1736 Jackson, M.G., Becker, T.W. & Konter, J.G. Geochemistry and distribution of recycled domains
1737 in the mantle inferred from Nd and Pb isotopes in oceanic hot spots: Implications for
1738 storage in the large low shear wave velocity provinces. *Geochem. Geophys. Geosystems*
1739 **19(9)**, 3496-3519 (2018).
1740 Jackson, M.G., Blichert-Toft, J., Halldórsson, S.A., Mundl-Petermeier, A., Bizimis, M., Kurz,
1741 M.D., Price, A.A., Hardardóttir, S., Willhite, L.N., Breddam, K., Becker, T.W. & Rischer,

R.A. Ancient helium and tungsten isotopic signatures preserved in mantle domains least modified by crustal recycling. *Proc. Natl. Acad. Sci. U.S.A.* **117**, 30993-31001 (2020a).
Jackson, M.G., Halldórsson, S.A., Price, A., Kurz, M.D., Konter, J.G., Koppers, A.A.P. & Day, J.M.D. Contrasting old and young volcanism from Aitutaki, Cook Islands: Implications for a hotspot origin. *J. Petrol.* **61(3)**, egaa037 (2020b).
Jacobsen, S.B., Wasserburg, G. J. The mean age of mantle and crustal reservoirs. *J. Geophys. Res. Solid Earth* **84**, 7411–7427 (1979).
Johnston, S., Brandon, A., McLeod, C. Rankenburg, K., Becker, H., Copeland, P. Nd isotope variation between the Earth–Moon system and enstatite chondrites. *Nature* **611,** 501-506 (2022).
Jones, T.D., Davies D.R., Campbell I.H., Wilson C.R. & Kramer S.C. Do mantle plumes preserve the heterogeneous structure of their deep-mantle source? *Earth Planet. Sci. Lett.* **434**, 10–17 (2016).
Jones, T.D., Davies, D.R., Campbell, I.H., Iaffaldano, G., Yaxley, G., Kramer, S.C. & Wilson, C.R. The concurrent emergence and causes of double volcanic hotspot tracks on the Pacific plate. *Nature*, **545**, 472-476 (2017).
Jones, T. D., Sime, N. & van Keken, P. E. Burying Earth's primitive mantle in the slab graveyard. *Geochem. Geophys. Geosystems* **22**, e2020GC009396 doi:10.1029/2020GC009396 (2021).
Karato, S. Rheology of the deep upper mantle and its implications for the preservation of the continental roots: a review. *Tectonophysics* **481**, 82–98 (2010).
Kelley, K.A., Plank, T., Farr, L., Ludden, J., & Staudigel, H. Subduction cycling of U, Th, and Pb. *Earth Planet. Sci. Lett.* **234**(3-4), 369-383 (2005).
Kerr, R. & Mériaux, C. Structure and dynamics of sheared mantle plumes. *Geochem. Geophys. Geosystems* **5,** 12 doi:10.1029/2004GC000749 (2004).
Kerr, B.C., Scholl, D.W. & Klemperer, S.L. Seismic stratigraphy of Detroit Seamount, Hawaiian-Emperor Seamount chain: Post-hot-spot shield-building volcanism and deposition of the Meiji drift. *Geochem. Geophys. Geosystems* **6 (7)**, Q07L10 (2005).
Kim, Y. et al. Structural Transitions in MgSiO3 Glasses and Melts at the Core-Mantle Boundary Observed via Inelastic X-ray Scattering. *Geophys. Res. Lett.* **46**, 13756–13764 (2019).
King, S.D. & Adam, C. Hotspot swells revisited. *Phys. Earth. Planet. Int.* **235**, 66-83 (2014).
Kingsley, R.H. & Schilling, J.-G. Plume-ridge interaction in the Easter-Salas y Gomez seamount chain – Easter Microplate system: Pb isotope evidence. *J. Geophys. Res.* **103**, 24,159 – 24,177 (1998).
Kingsley, R.H., Blichert-Toft, J., Fontignie, D. & Schilling, J.-G. Hafnium, neodymium, and strontium isotope and parent-daughter element systematics in basalts from the plume-ridge interaction system of the Salas y Gomez Seamount Chain and Easter Microplate. *Geochem. Geophys. Geosyst.* **8**, Q04005 (2007).
Kleine T, Münker C, Mezger K & Palme H. Rapid accretion and early core formation on asteroids and the terrestrial planets from Hf-W chronometry. *Nature* **418**, 952–955. (doi:10.1038/nature00982) (2002).
Knittle E. & Jeanloz, R. Melting curve of (Mg,Fe)SiO3 perovskite to 96 GPa: Evidence for a structural transition in lower mantle melts, *Geophys. Res. Lett.* **16**, 421-424 (1989).
Kobayashi, K., Tanaka, R., Moriguti, T., Shimizu, K. & Nakamura, E. Lithium, boron, and lead isotope systematics of glass inclusions in olivines from Hawaiian lavas: evidence for recycled components in the Hawaiian plume. *Chem. Geol.* **212**, 143-161 (2004).

Koelemeijer P., Ritsema J., Deuss A., van Heijst H.-J. SP12RTS: a degree-12 model of shear- and compressional-wave velocity for Earth's mantle. *Geophys. J. Int.* **204**, 1024-103 (2016).

Konter, J.G. & Jackson, M.G. Large volumes of rejuvenated volcanism in Samoa: Evidence supporting tectonic influence on late-stage volcanism. *Geochem. Geophys. Geosystems* **13(1)**, Q0AM04 (2012).

Koppers, A.A.P., Becker, T.W., Jackson, M.G., Konrad, K., Muller, R.D., Romanowicz, B., Steinberger, B. & Whittaker, J.M. Mantle plumes and their role in Earth processes. *Nature Reviews Earth & Environment* **2**, 382–401 (2021).

Korenaga, J. Firm mantle plumes and the nature of the core-mantle boundary region. *Earth Planet. Sci. Lett.* **232**, 29–37 (2005).

Krienitz M. S., Garbe-Schonberg C. D., Romer R. L., Meixner A., Haase K. M. & Stroncik N. A. Lithium isotope variations in ocean island basalts – implications for the development of mantle heterogeneities. *J. Petrol.* **53**, 2333–2347 (2012).

Kruijer, T.S. & Kleine, T. No W-182 excess in the Ontong Java Plateau source. *Chem. Geol.* **485**, 24-31 DOI10.1016/j.chemgeo.2018.03.024 (2018).

Kumagai, I., Davaille, A., Kurita, K. & Stutzmann, E. Mantle plumes: Thin, fat, successful, or failing? Constraints to explain hot spot volcanism through time and space. *Geophys. Res. Lett.* **35**, L16301 (2008).

Labrosse, S., Hernlund, J.W. & Coltice, N. A crystallizing dense magma ocean at the base of the Earth's mantle. *Nature* **450**, 866-869 (2007).

Lee, C.T.A., Luffi, P., Hoink, T., Li, J., Dasgupta, R., Hernlund, J. Upside-down differentiation and generation of a 'primordial' lower mantle. *Nature* **463**, 930-933 DOI10.1038/nature08824 (2010).

Lee, K.K.M., O'Neill, B., Panero, W.R., Shim, S.H., Benedetti, L.R., Jeanloz, R. Equations of state of the high-pressure phases of a natural peridotite and implications for the Earth's lower mantle. *Earth Planet. Sci. Lett.* **223**, 3–4, 381-393, doi.org/10.1016/j.epsl.2004.04.033 (2004).

Li, M., McNamara, A.K. & Garnero, E.J. Chemical complexity of hotspots caused by cycling oceanic crust through mantle reservoirs. *Nat. Geosci.* **7**, 366-370 (2014).

Limare, A., Jaupart, C., Kaminski, E., Fourel, L. & Farnetani C.G. Convection in an internally heated stratified heterogeneous reservoir. *J. Fluid Mech.* **870**, 67–105 doi:10.1017/jfm.2019.243 (2019).

Lin, S.C. & van Keken, P.E. Dynamics of thermochemical plumes: 2. Complexity of plume structures and its implications for mapping mantle plumes. *Geochem. Geophys. Geosystems* **7(3)**, Q03003. (2006).

Litasov, K.D., & Ohtani, E. Effect of water on the phase relations in Earth's mantle and deep water cycle, *in* Ohtani, E., ed., Advances in High-Pressure Mineralogy: *Spec. Pap. Geol. Soc. Am.* **421**, p. 115–156, doi: 10.1130/2007.2421(08) (2007).

Lock, S. J., Bermingham, K. R., Parai, R. & Boyet, M. Geochemical Constraints on the Origin of the Moon and Preservation of Ancient Terrestrial Heterogeneities. *Space Sci. Rev.* **216**, 109 (2020).

Macdonald, G.A. & Katsura, T. Chemical composition of the Hawaiian lavas. *J. Petrol*. **5**, 82-133 (1964).

1832 Manhès, G., Minster, J. F. & Allègre, C. J. Comparative uranium-thorium-lead and rubidium-
1833 strontium study of the Saint Sèverin amphoterite: consequences for early solar system
1834 chronology. *Earth Planet Sc Lett* **39**, 14–24 (1978).
1835 Manga, T., Wiechert, U., Stuart, F.M., Halliday, A.N. & Harrison, D. Combined Li-He isotopes
1836 on Iceland and Jan Mayen basalts and constraints on the nature of the North Atlantic
1837 mantle. *Geochem. Cosmochim. Acta* **75**, 922-936 (2011).
1838 Mao, W.L., Mao, H-K., Sturhahn, W., Zhao, J., Prakapenka, V.B., Meng, Y., Shu, J., Fei, Y.,
1839 Russell J., Hemley R.J. Iron-Rich Post-Perovskite and the Origin of Ultralow-Velocity
1840 Zones, *Science*, **312**, 564-565 (2006).
1841 Marschall, H.R., Wanless, V.D., Shimizu, N., Pogge von Strandmann, P.A.E., Elliott, T. &
1842 Monteleone, B.D. The boron and lithium isotopic composition of mid-ocean ridge basalts
1843 and the mantle. *Geochim. Cosmochim. Acta* **207**, 102-138 (2017).
1844 Masters, G., Laske, G., Bolton, H. & Dziewonski, A. The relative behavior of shear velocity,
1845 bulk sound speed, and compressional velocity in the mantle: Implications for chemical and
1846 thermal structure. *Geophys. Monogr. Ser.* **117**, 63–87 (2000).
1847 McDonough, W.F. & Chauvel, C. Sample Contamination Explains the Pb Isotopic Composition
1848 of Some Rurutu Island and Sasha Seamount Basalts. *Earth Planet. Sci. Lett.* **105**, 397–404
1849 (1991).
1850 McDonough, W.F. & Sun, S. -s. The composition of the Earth. *Chem. Geol.* **120**, 223–253
1851 (1995).
1852 McDonough, W.F. The Composition of the Lower Mantle and Core. *Deep Earth: Physics and*
1853 *Chemistry of the Lower Mantle and Core, Geophysical Monograph* **217**. 145-159. Edited
1854 by H. Terasaki and R.A. Fischer. AGU, John Wiley & Sons, Inc (2016).
1855 McNamara, A.K. A review of large low shear velocity provinces and ultra-low velocity zones.
1856 *Tectonophysics* **760**, 199–220 (2019).
1857 Montelli, R., Nolet, G., Dahlen, F.A. & Masters, G. A catalog of deep mantle plumes: New
1858 results from finite frequency tomography. *Geochem. Geophys. Geosystems* **7(11)**, Q11007
1859 (2006).
1860 Morgan, W. . Convection plumes in the lower mantle. *Nature* **230**, 42–43 (1971).
1861 Moreira, M., Kunz, J. & Allègre, C. Rare gas systematics in popping rock: Isotopic and
1862 elemental compositions in the upper mantle. *Science* **279, 5354** 1178-1181
1863 DOI10.1126/science.279.5354.1178 (1998).
1864 Moreira, M., Doucelance, R., Kurz, M.D., Dupré, B. & Allègre, C.J. Helium and lead isotope
1865 geochemistry of the Azores Archipelago. *Earth Planet. Sci. Lett.* **169,** 189-205
1866 DOI10.1016/S0012-821X(99)00071-0 (1999).
1867 Morino, P., Caro, G., Reisberg, L. & Schumacher, A. Chemical stratification in the post-magma
1868 ocean Earth inferred from coupled 146,147Sm–142,143Nd systematics in ultramafic rocks
1869 of the Saglek block (3.25–3.9 Ga; northern Labrador, Canada). *Earth Planet. Sci. Lett.* **463**,
1870 136–150 (2017).
1871 Morris, J., Valentine, R. & Harrison, T. 10Be imaging of sediment accretion and subduction
1872 along the northeast Japan and Costa Rica convergent margins. *Geology* **30(1)**, 59-62
1873 (2002).
1874 Mukhopadhyay, S. Early differentiation and volatile accretion recorded in deep-mantle neon and
1875 xenon. *Nature* **486**, 101-104, doi:10.1038/nature11141 (2012).

Mundl, A., Touboul, M., Jackson, M.G., Day, J.M.D., Kurz, M.D., Lekic, V., Helz, R.T. & Walker, R.J. Tungsten-182 heterogeneity in modern ocean island basalts. *Science*, **356,** 66-69 (2017).

Mundl-Petermeier, A., Walker, R.J., Jackson, M.G., Blichert-Toft, J., Kurz, M.D. & Halldorsson, S.A. Temporal evolution of primordial tungsten-182 and He-3/He-4 signatures in the Iceland mantle plume. *Chem. Geol.* **525,** 245-259 DOI10.1016/j.chemgeo.2019.07.026 (2019).

Mundl-Petermeier, A., Walker, R.J., Fischer, R.A., Lekic, V., Jackson, M.G. & Kurz, M.D. Anomalous 182W in high 3He/4He ocean island basalts: Fingerprints of Earth's core? *Geochim. Cosmochim. Acta* **71**, 194–211 (2020).

Murphy DT., A. D. Brandon, V. Debaille, R. Burgess, C. Ballentine, In search of a hidden long-term isolated sub-chondritic $^{142}Nd/^{144}Nd$ reservoir in the deep mantle: Implications for the Nd isotope systematics of the Earth. *Geochim. Cosmochim. Acta* **74**, 738–750 (2010)

Nakagawa, T., Tackley, P.J., Deschamps, F. & Connolly, J.A.D. Incorporating self-consistently calculated mineral physics into thermochemical mantle convection simulations in a 3-D spherical shell and its influence on seismic anomalies in Earth's mantle. *Geochem. Geophys. Geosystems* **10**, Q03004 DOI10.1029/2008GC002280 (2009).

Nakagawa, T. & Tackley, P.J. Influence of combined primordial layering and recycled MORB on the coupled thermal evolution of Earth's mantle and core. *Geochem. Geophys. Geosystems* **15**, 619–633 doi:10.1002/2013GC005128 (2014).

Newsom, H.E., White, W.M., Jochum, K.P. & Hofmann, A.W. Siderophile and chalcophile element abundances in oceanic basalts, Pb isotope evolution and growth of the Earth's core. *Earth Planet. Sci. Lett.* **80**, 299-313 (1986).

Nielsen, S.G., Rehkämper, M., Teagle, D.A., Butterfield, D.A., Alt, J.C. & Halliday, A.N. Hydrothermal fluid fluxes calculated from the isotopic mass balance of thallium in the ocean crust. *Earth Planet. Sci. Lett.* **251(1)**, 120-133 (2006a).

Nielsen, S.G., Rehkämper, M., Norman, M.D., Halliday, A.N. & Harrison, D. Thallium isotopic evidence for ferromanganese sediments in the mantle source of Hawaiian basalts. *Nature* **439,** 314-317 (2006b).

Nielsen, S.G., Rehkämper, M. & Prytulak, J. Investigation and application of thallium isotope fractionation. *Rev. Mineral. Geochem.* **82(1)**, 759-798 (2017).

Nishio, Y., Nakai, S., Yamamoto, J., Sumino, H., Matsumoto, T., Prikhod'ko, V. & Arai, S. Lithium isotopic systematics of the mantle-derived ultramafic xenoliths: implications for EM1 origin. *Earth Planet. Sci. Lett.* **217**, 245-261 (2004).

Nobre Silva I., Weis D., Barling J., Scoates J.S. Basalt leaching systematics and consequences for Pb isotopic compositions by MC-ICP-MS. *Geochem. Geophys. Geosystems* **10**, Q08012, doi:10.1029/2009GC002537 (2009).

Nobre Silva I.G., Weis D., Scoates J.S. Effects of acid leaching on the Sr-Nd-Hf isotopic compositions of ocean island basalts. *Geochem. Geophys. Geosystems* **11**, Q09011, doi: 10.1029/2010GC003176, (2010).

Nobre Silva I., Weis D., Scoates J. Isotopic systematics of the early Mauna Kea shield phase and insight into the deep mantle beneath the Pacific Ocean. *Geochem. Geophys. Geosystems* **14**, 659-676, doi:10.1002/ggge.20047 (2013a).

Nobre-Silva, I. G. N., Weis, D., Scoates, J. S. & Barling, J. The Ninetyeast Ridge and its Relation to the Kerguelen, Amsterdam and St. Paul Hotspots in the Indian Ocean. *J. Petro*l. **54**, 1177–1210 (2013b).

Olson, P., Schubert, G. & Anderson C. Structure of axisymmetric mantle plumes. *J. Geophys. Res*. **98**, 6829-6844 (1993).
Olson, P.L. & Sharp, Z.D. Primordial helium-3 exchange between Earth's core and mantle. *Geochem. Geophys. Geosystems* **23**, e2021GC009985 (2022).
O'Neil, J., Carlson, R.W., Francis, D. & Stevenson, R.K. Neodymium-142 evidence for hadean mafic crust. *Science* **321**, 1828-1831 DOI10.1126/science.1161925 (2008).
O'Nions, R.K., Evensen, N.M. & Hamilton, P.J. Geochemical modeling of mantle differentiation and crustal growth. *J. Geophys. Res. Solid Earth* **84**, 6091–6101 (1979).
Parai, R., Mukhopadhyay, S. & Standish, J.J. Heterogeneous upper mantle Ne, Ar and Xe isotopic compositions and a possible Dupal noble gas signature recorded in basalts from the Southwest Indian Ridge. *Earth Planet. Sci. Lett.* **359**, 227-239, doi:10.1016/j.epsl.2012.10.017 (2012).
Parai, R. & Mukhopadhyay, S. The evolution of MORB and plume mantle volatile budgets: Constraints from fission Xe isotopes in Southwest Indian Ridge basalts. *Geochem. Geophys. Geosystems* **16,** 719-735 DOI10.1002/2014GC005566 (2015).
Parai, R. & Mukhopadhyay, S. Xenon isotopic constraints on the history of volatile recycling into the mantle. *Nature* **560**, 223-227 (2018).
Parai, R., Mukhopadhyay, S., Tucker, J.M. & Pető, M.K. The emerging portrait of an ancient, heterogeneous and continuously evolving mantle plume source. *Lithos* **346-347**, 105153, doi:https://doi.org/10.1016/j.lithos.2019.105153 (2019).
Parai, R., & Mukhopadhyay, S. Heavy noble gas signatures of the North Atlantic Popping Rock 2 Pi D43: Implications for mantle noble gas heterogeneity. *Geochim. Cosmochim. Acta* **294**, 89-105 DOI10.1016/j.gca.2020.11.011 (2021).
Parai, R. A dry ancient plume mantle from noble gas isotopes. *Proc. Natl. Acad. Sci. U.S.A.* **119**(29), doi.org/10.1073/pnas.2201815119 (2022).
Payne, J.A., Jackson, M.G. & Hall, P.S. Parallel volcano trends and geochemical asymmetry of the Society hotspot track. *Geology* **41(1)**, 19-22 (2013).
Pearce, J.A., Ernst, R.E., Peate, D.W. & Rogers, C. LIP printing: Use of immobile element proxies to characterize Large Igneous Provinces in the geologic record. *Lithos* **392-393**, 106068 (2021).
Penniston-Dorland S., Liu X.-M. & Rudnick R.L. Lithium isotope geochemistry. *Rev. Mineral. Geochem.* **82**, 165-217 (2017).
Péron, S. & Moreira, M. Onset of volatile recycling into the mantle determined by xenon anomalies. *Geochem. Perspect. Lett.* **9**, 21-25 (2018).
Péron, S., Mukhopadhyay, S., Kurz, M.D. & Graham, D.W. Deep-mantle krypton reveals Earth's early accretion of carbonaceous matter. *Nature* **600**, 462-467 (2021).
Peters, B.J., Carlson, R.W., Day, J.M.D. & Horan, M.F. Hadean silicate differentiation preserved by anomalous Nd-142/Nd-144 ratios in the Reunion hotspot source. *Nature* **555**, 89-93 DOI10.1038/nature25754 (2018).
Peters, B.J., Mundl-Petermeier, A., Carlson, R.W., Walker, R.J. & Day, J.M.D. Combined Lithophile-Siderophile Isotopic Constraints on Hadean Processes Preserved in Ocean Island Basalt Sources. *Geochem. Geophys. Geosystems* **22**, DOI10.1029/2020GC009479 (2021).
Pető, M. K., Mukhopadhyay, S. & Kelley, K. A. Heterogeneities from the first 100 million years recorded in deep mantle noble gases from the Northern Lau Back-arc Basin. *Earth Planet. Sci. Lett.* **369**, 13-23, doi:10.1016/j.epsl.2013.02.012 (2013).

Plank, T. & Langmuir, C.H. The chemical composition of subducting sediment and its consequences for the crust and mantle. *Chem. Geol.* **145** 325-394 (1998).

Porcelli, D. & Halliday, A. The core as a possible source of mantle helium. *Earth Planet. Sci. Lett.* **192**, 45–56 (2001).

Porter, K.A. & White, W.M. Deep mantle subduction flux. *Geochem. Geophys. Geosystems* **10(12)** Q12016 (2009).

Puchtel, I.S., Blichert-Toft, J., Touboul, M., Horan, M.F. & Walker, R.J. The coupled W-182-Nd-142 record of early terrestrial mantle differentiation. *Geochem. Geophys. Geosystems* **17**, 2168-2193 DOI10.1002/2016GC006324 (2016).

Putirka, K.D., Perfit, M., Ryerson, F.J. & Jackson, M.G. Ambient and excess mantle temperatures, olivine thermometry, and active vs. passive upwelling. *Chem. Geol*. **241**, 177-206 (2007).

Putirka, K. Excess temperatures at ocean islands: Implications for mantle layering and convection. *Geology* **36**, 283-286 (2008).

Ravizza, G., Blusztajn, J. & Prichard, H.M. Re-Os systematics and platinum-group element distribution in metalliferous sediments from the Troodos ophiolite. *Earth Planet. Sci. Lett.* **188**, 369-381 DOI10.1016/S0012-821X(01)00337-5 (2001).

Regelous, M., Hofmann, A.W., Abouchami, W. & Galer, S.J.G. Geochemistry of lavas from the Emperor Seamounts, and the geochemical evolution of Hawaiian magmatism from 85 to 42 Ma. *J. Petrol.* **44**, 113-140 DOI10.1093/petrology/44.1.113 (2003).

Rehkämper, M., Frank, M., Hein, J. R., Porcelli, D., Halliday, A., Ingri, J. & Liebetrau, V. Thallium isotope variations in seawater and hydrogenetic, diagenetic, and hydrothermal ferromanganese deposits. *Earth Planet. Sci. Lett.* **197(1)**, 65-81 (2002).

Richards, M.A., Duncan, R.A. & Courtillot, V.E. Flood basalts and hotspot tracks: Plume heads and tails, *Science* **246**, 103--107, 1989.

Ricolleau, A., Perrillat, J.-P., Fiquet, G., Daniel, I., Matas, J., Addad, A., Menguy, N., Cardon, H., Mezouar, M., & Guignot, N. Phase relations and equation of state of a natural MORB: Implications for the density profile of subducted oceanic crust in the Earth's lower mantle. *J. Geophys. Res.* **115**, B08202. https://doi.org/10.1029/2009JB006709 (2010).

Ritsema, J. & Lekic, V. Heterogeneity of seismic wave velocity in Earth's mantle. *Ann. Rev. Earth Planet. Sci.* **48**, 377-401 (2020).

Rizo, H., Walker, R.J., Carlson, R. W., Horan, M.F., Mukhopadhyay, S., Manthos, V., Francis, D. & Jackson, M.G. Preservation of Earth-forming events in the tungsten isotopic composition of modern flood basalts. *Science* **352**, 809–812 (2016).

Rizo, H., Andrault, D., Bennett, N.R., Humayun, M., Brandon, A., Vlastelic, I., et al. ^{182}W evidence for core-mantle interaction in the source of mantle plumes. *Geochem. Perspect. Lett.* **11**, 6–11. https://doi.org/10.7185/geochemlet.191 (2019).

Rohde, J., Hoernle, K., Hauff, F., Werner, R., O'Connor, J., Class, C., Garbe-Schönberg, D. & Jokat, W. 70 Ma chemical zonation of the Tristan-Gough hotspot track. *Geology* **41(3)**, 335–338 (2013).

Roth, A.S.G., Bourdon, B., Mojzsis, S.J., Rudge, J.F., Guitreau, M. Blichert-Toft, J. Combined Sm-147, Sm-146-Nd-143, Nd-142 constraints on the longevity and residence time of early terrestrial crust. *Geochem. Geophys. Geosystems* **15(6)**, 2329-2345 DOI10.1002/2014GC005313 (2014).

Roth, A.S.G., Liebske, C., Maden, C., Burton, K.W., Schonbachler, M. & Busemann, H. The primordial He budget of the Earth set by percolative core formation in planetesimals. *Geochem. Perspect. Lett* **9,** 26–31 (2019).

Rudge, J.F., Maclennan, J. & Stracke, A. The geochemical consequences of mixing melts from a heterogeneous mantle. *Geochim. Cosmochim. Acta*, **114**, 112-143 (2013).

Rudnick, R.L. & Gao, S. Composition of the Continental Crust. In: Editors-in-Chief: Heinrich, D.H., Karl, K.T. (Eds.), Treatise on Geochemistry. Pergamon, Oxford, pp. 1-64 (2003).

Ryan, J.G. & Kyle, P.R. Lithium abundance and lithium isotope variaitons in mantle sources: insights from intraplate volcanic rocks from Ross Island and Marie Byrd Land (Antarctica) and other oceanic islands. *Chem. Geol.* **212**, 125-142 (2004).

Ryan, J.G. & Chauvel, C., The Subduction-Zone Filter and the Impact of Recycled Materials on the Evolution of the Mantle. In: Holland, H.D., Turekian, K.K. (Eds.), *Treatise on Geochemistry* (Second Edition). Elsevier, Oxford, pp. 479-508 (2014).

Saal, A.E., Hart, S.R., Shimizu, N., Hauri, E.H., Layne, G.D. Pb isotopic variability in melt inclusions from the EMI–EMII–HIMU mantle end-members and the role of the oceanic lithosphere. *Earth Planet Sc Lett.* **240**, 605–620 (2005).

Saji N.K., Wielandt D., Paton C., Bizzaro M. Ultra-high-precision Nd-isotope measurements of geological materials by MC-ICPMS. *J. Anal. At.Spectrom.* **31**, 1490-1504 (2016).

Saji N.S., K. Larsen, D. Wielandt, M. Schiller, M.M. Costa, M.J. Whitehouse, M.T. Rosing, M. Bizzarro, Hadean geodynamics inferred from time-varying in the early Earth rock record $^{142}Nd/^{144}Nd$ in the early Earth rock record. *Geochem. Perspect. Lett.* **7**,43–48 (2018).

Salters, V.J.M. & Stracke, A. Composition of the depleted mantle. *Geochem. Geophys. Geosystems* **5**, Q0500 DOI10.1029/2003GC000597 (2004).

Schilling, J.G., Kingsley, R.H., & Devine, J.D. Galápagos hot spot-spreading center system: 1. Spatial petrological and geochemical variations (83oW–101oW). *J. Geophys. Res. Solid Earth*, **87(B7)**, 5593-5610 (1982).

Schilling, J-G. Fluxes and excess temperatures of mantle plumes inferred from their interaction with migrating mid-ocean ridges. *Nature* **352**, 397–403 (1991).

Schuessler, J.A., Schoenberg, R. & Sigmarsson, O. Iron and lithium isotope systematics of the Heckla volcano, Iceland - Evidence for Fe isotope fractionation during magma differentiation. *Chem. Geol.* **258**, 78-91 (2009).

Shahar, A., Hillgren, VJ., Young, E.D., Fei, Y., Macris, C.A., Deng L. High-temperature Si isotope fractionation between iron metal and silicate. *Geochim. Cosmochim. Acta* **75** (23), 7688-7697 (2011).

Shahar, A., Schauble, E.A., Caracas, R., Gleason, A.E., Reagan, M.M., Xiao, Y., Shu, J. & Mao, W. Pressure-dependent isotopic composition of iron alloys. *Science* **352**, 580-582 DOI10.1126/science.aad9945 (2016).

Shahar, A., Elardo, S.M. & Macris, C.A. Equilibrium Fractionation of Non-Traditional Stable Isotopes: An Experimental Approach, *Rev. Min. Geoch.,* **82**, 65-84 (2017).

Sleep, N.H. Hotspots and mantle plumes: Some phenomenology. *J. Geophys. Res. Solid Earth* **95**, 6715-6736 (1990).

Smith, E. M., Ni, P., Shirey, S. B., Richardson, S. H., Wang, W. & Shahar, A. Heavy iron in large gem diamonds traces deep subduction of serpentinized ocean floor. *Sci. Adv.* **7(14)**, eabe9773 (2021).

Stracke, A., Hofmann, A.W. & Hart, S.R. FOZO, HIMU, and the rest of the mantle zoo. *Geochem. Geophys. Geosystems* **6(5)**, Q05007 (2005).

Stracke, A., Bourdon, B. & McKenzie, D. Melt extraction in the Earth's mantle: Constraints from U-Th-Pa-Ra studies in oceanic basalts. *Earth Planet. Sci. Lett.* **244**, 97-112 DOI10.1016/j.epsl.2006.01.057 (2006).

Stracke, A. Earth's heterogeneous mantle: A product of convection-driven interaction between crust and mantle. *Chem. Geol.* **330–331(0)** 274-299 (2012).

Stracke, A., Willig, M., Genske, F., Béguelin, P. & Todd, E. Chemical Geodynamics Insights From a Machine Learning Approach. *Geochem. Geophys. Geosystems* **23**, e2022GC010606 (2022).

Stuart, F.M., Lass-Evans, S., Fitton, J.G. & Ellam, R.M. High He-3/He-4 ratios in picritic basalts from Baffin Island and the role of a mixed reservoir in mantle plumes. *Nature* **424**, 57-59 DOI10.1038/nature01711 (2003).

Tackley, P.J. Three-dimensional simulations of mantle convection with a thermo-chemical basal boundary layer: D" ?, in The Core-Mantle Boundary Region, *Geophys. Monogr. Ser.*, **28**, edited by M. Gurnis et al., pp. 231 – 253, AGU, Washington, D. C. (1998).

Tang, M., Rudnick, R.L. & Chauvel, C. Sedimentary input to the source of Lesser Antilles lavas: A Li perspective. *Geochim. Cosmochim. Acta* **144**, 43-58 (2014).

Thorne, M.S. & Garnero, E.J. Inferences on ultralow-velocity zone structure from a global analysis of SPdKS waves. *J. Geophys. Res. Solid Earth* **109** http://dx.doi.org/10.1029/2004jb003010 (2004).

Tkalčić, H., Young, M., Muir, J. B., Davies, D.R. & Mattesini, M. Strong, multi-scale heterogeneity in Earth's lowermost mantle. *Sci. Rep.* **5**, 18416, doi:10.1038/srep18416 (2015).

Tomascak, P.B. Developments in the understanding and application of lithium isotopes in the earth and planetary sciences. *Rev. Mineral. Geochem.* **55(1)**, 153-195 10.2138/gsrmg.55.1.153 (2004).

Tomascak, P.B., Langmuir, C.H., le Roux, P.J. & Shirey, S.B. Lithium isotopes in global mid-ocean ridge basalts. *Geochim. Cosmochim. Acta*, **72**, 1626-1637 (2008).

Torsvik, T.H., Smethurst, M. A., Burke, K. & Steinberger, B. Large igneous provinces generated from the margins of the large low-velocity provinces in the deep mantle. *Geoph. J. Int.* **167**, 1447-1460 doi:10.1111/j.1365-246X.2006.03158.x (2006).

Touboul, M., Puchtel, I.S. & Walker, R.J. W-182 evidence for long-term preservation of early mantle differentiation products. *Science* **335**, 1065-1069 DOI10.1126/science.1216351 (2012a).

Touboul, M. & Walker, R. J. High precision tungsten isotope measurement by thermal ionization mass spectrometry. *Int. J. Mass Spectrom.* **309**, 109–117 (2012b).

Trinquier A., Touboul M., Walker R.J. High-Precision Tungsten Isotopic Analysis by Multicollection Negative Thermal Ionization Mass Spectrometry Based on Simultaneous Measurement of W and 18O/16O Isotope Ratios for Accurate Fractionation Correction. *Anal. Chem.* **88**, 1542-1546 (2016).

Tronnes, R.G., Baron, M.A., Eigenmann, K.R., Guren, M.G., Heyn, B.H., Loken, A. & Mohn, C.E. Core formation, mantle differentiation, and core-mantle interaction within Earth and terrestrial planets. *Tectonophysics* **760**, 165-198 (2019).

Tschauner, O., Ma, C., Beckett, J.R., Prescher, C., Prakapenka, V.B., & Rossman, G.R. Discovery of bridgmanite, the most abundant mineral in Earth, in a shocked meteorite. *Science*, **346**(6213), 1100–1102. https://doi.org/10.1126/science.1259369 (2014).

Tucker, J. M., Mukhopadhyay, S. & Schilling, J.-G. The heavy noble gas composition of the depleted MORB mantle (DMM) and its implications for the preservation of heterogeneities in the mantle. *Earth Planet. Sci. Lett.* **355–356**, 244–254 (2012).

Turner, S., Bourdon, B. & Gill, J. Insights into magma genesis at convergent margins from U-series isotopes. *Rev. Mineral. Geochem.* **52**, 255-315 (2003).

Turner, S.J. & Langmuir, C.H. Sediment and ocean crust both melt at subduction zones. *Earth Planet. Sc. Lett.* **584**, 117424 (2022).

Upadhyay D., Scherer E.E., Mezger K. Fractionation and mixing of Nd isotopes during thermal ionization mass spectrometry: implications for high precision $^{142}Nd/^{144}Nd$ analyses. *J. Anal. At. Spec.* **23**, 561-568 (2008).

Vervoort, J.D., Patchett, P.J., Blichert-Toft, J. & Albarède, F. Relationships between Lu-Hf and Sm-Nd isotopic systems in the global sedimentary system. *Earth Planet. Sci. Lett* **168,**79-99 DOI10.1016/S0012-821X(99)00047-3 (1999).

Vlastélic, I., Koga, K., Chauvel, C., Jaques, G. & Télouk, P. Survival of lithium isotopic heterogeneities in the mantle supported by HIMU-lavas from Rurutu Island, Austral Chain. *Earth Planet. Sci. Lett.* **286(3-4)**, 456-466 (2009).

Walker, R.J. Siderophile element constraints on the origin of the Moon. *Phil. Trans. Roy. Soc. A. London,* **372**, 2024 DOI10.1098/rsta.2013.0258 (2014).

Wamba, M.D., Montagner, J.-P. & Romanowicz, B. Imaging deep-mantle plumbing beneath La Réunion and Comores hot spots: Vertical plume conduits and horizontal ponding zones. *Sci Adv* **9**, eade3723 (2023).

Wang, X.-J. et al. Recycled ancient ghost carbonate in the Pitcairn mantle plume. *Proc. National Acad. Sci.* **115**, 8682–8687 (2018).

Weaver, B.L. The origin of ocean island basalt end-member compositions: trace element and isotopic constraints. *Earth Planet. Sci. Lett*. **104**, 381-397 (1991).

Weis, D., Bassias, Y., Gautier, I. & Mennessier, J.-P. Kerguelen Plateau (South Indian Ocean): Isotopic study of MD48 dredge basalts: Kerguelen type signature. *Geochim. Cosmochim. Acta* ***53*****,** 2125-2131 (1989).

Weis, D. & Frey, F.A. Submarine basalts of the Northern Kerguelen Plateau: Interaction between the Kerguelen plume and the Southeast Indian Ridge revealed at ODP Site 1140. *J. Petrol*. **43**, 1287-1309 (2002).

Weis, D., Kieffer, B., Maerschalk, C., Barling, J., De Jong, J., Williams, G.A., Hanano, D., Pretorius, W., Mattielli, N., Scoates, J.S., Goolaerts, A., Friedman, R.M., Mahoney, J.B. High-precision isotopic characterization of USGS reference materials by TIMS and MC-ICP-MS. *Geochem. Geophys. Geosystems* **7**, Q08006 (2006).

Weis, D., Kieffer, B., Hanano, D., Nobre Silva, I., Barling, J., Pretorius, W., Maerschalk, C., Mattielli, N. Hf isotope compositions of U.S. Geological Survey reference materials. *Geochem. Geophys. Geosystems* **8(6)**, Q06006 (2007).

Weis, D., Garcia, M. O., Rhodes, J. M., Jellinek, M. & Scoates, J. S. Role of the deep mantle in generating the compositional asymmetry of the Hawaiian mantle plume. *Nat. Geosci.* **4**, 831–838 (2011).

Weis D., Harrison L., McMillan R. & Williamson N.W.B. Fine-scale structure of Earth's deep mantle resolved through statistical analysis of Hawaiian basalt geochemistry. *Geochem. Geophys. Geosystems* **21**, e2020GC009292. https://doi.org/10.1029/2020GC009292 (2020).

Weiss, Y., Class, C., Goldstein, S.L. & Hanyu, T. Key new pieces of the HIMU puzzle from olivines and diamond inclusions. *Nature* **537**, 666-670 (2016).
Wessel, P., & Kroenke, L.W. Observations of geometry and ages constrain relative motion of Hawaii and Louisville plumes. *Earth Planet. Sci. Lett.* **284**(3-4), 467-472 (2009).
Wessel, P. Regional–residual separation of bathymetry and revised estimates of Hawaii plume flux. *Geophys. Jour. Int.* **204**, 932–947 (2016).
Wetherill, G. W. Radiometric Chronology of the Early Solar System. *Ann. Rev. Nucl. Sci.* **25**, 283–328 (1975).
White, R.S. & McKenzie, D.P. Volcanism at rifts. *Sci. Am.* **261(1)**, 62-71 (1989).
White, R.S. Melt production rates in mantle plumes. *Phil. Trans. Roy. Soc. London* **342**, 137-153 (1993).
White, W.M., Schilling, J.-G. & Hart, S.R. Evidence for the Azores mantle plume from strontium isotope geochemistry of the Central North Atlantic. *Nature* **263**, 659–663 (1976).
White, W.M. Sources of oceanic basalts: Radiogenic isotopic evidence. *Geology* **13**, 115-118 (1985).
White, W.M., McBirney, A.R., & Duncan, R.A. Petrology and geochemistry of the Galápagos Islands: Portrait of a pathological mantle plume. *J. Geophys. Res. Solid Earth* ***98***(B11), 19533-19563 (1993).
White, W.M. & Duncan, R.A. Geochemistry and geochronology of the Society Islands: New evidence for deep mantle recycling. In: Basu, A. & Hart, S. (Ed.), *Earth Processes reading the isotopic code*. American Geophysical Union, Washington, pp. 183-206 (1996).
White, W.M. Oceanic island basalts and mantle plumes: the geochemical perspective. *Ann. Rev. Earth Planet. Sci.* **38**, 133-160 (2010).
White, W.M. Probing the Earth's deep interior through geochemistry. *Geochem. Perspect.* **4(2)**, 95-251 (2015).
Whitehead, J.A. & Luther, D.S. Dynamics of laboratory diapir and plume models. *J. Geophys. Res. Solid Earth* **80,** 705–717 (1975).
Willbold, M. & Stracke, A. Trace element composition of mantle end-members: Implications for recycling of oceanic and upper and lower continental crust. *Geochem. Geophys. Geosystems* **7**, Q04004 (2006).
Williams, C.D., Li, M., McNamara, A.K., Garnero, E.J. & van Soest, M.C. Episodic entrainment of deep primordial mantle material into ocean island basalts. *Nat. Comm.* **6**, 1-7 (2015).
Williams, C.D., Mukhopadhyaya, S., Rudolph, M.L. & Romanowitcz, B. Primitive helium is sourced from seismically slow regions in the lowermost mantle. *Geochem. Geophys. Geosystems* **20**, 4130-4145 (2019).
Williams, Q. & Garnero, E.J. Seismic evidence for partial melt at the base of Earth's mantle. *Science* **273**, 1528–1530 (1996).
Williamson N.M.B., Weis D., Scoates J.S., Pelletier H. & Garcia M.O. Tracking the geochemical transition between the Kea-Dominated Northwest Hawaiian Ridge and the bilateral Loa-Kea Trends of the Hawaiian Islands. *Geochem. Geophys. Geosystems* **20** DOI: 10.1029/2019GC008451, 4354-4369 (2019).
Williamson, N.M.B., Weis, D. & Prytulak, J. Thallium isotopic compositions in Hawaiian lavas: Evidence for recycled materials on the Kea side of the Hawaiian mantle plume. *Geochem. Geophys. Geosystems* **22(9)** e2021GC009765, https://doi.org/10.1029/2021GC009765 (2021).

Workman, R.K., Hart, S.R., Jackson, M., Regelous, M., Farley, K.A., Blusztajn, J., Kurz, M. & Staudigel, H. Recycled metasomatized lithosphere as the origin of the enriched mantle II (EM2) end-member: Evidence from the Samoan volcanic chain. *Geochem. Geophys. Geosystems* **5**, Q04008 DOI10.1029/2003GC000623 (2004).

Workman, R. & Hart, S. Major and trace element composition of the depleted MORB mantle (DMM). *Earth Planet. Sci. Lett.* **231**, 53–72 (2005).

Yamazaki, D., Kato, T., Yurimoto, H., Ohtani, E. & Toriumi, M. Silicon self-diffusion in MgSiO3 perovskite at 25 GPa. *Phys. Earth Planet. Inter.* **119**, 299–309 (2000).

Yang, H., Frey, F.A., Weis, D., Giret, A. Pyle, D. Michon, G. Petrogenesis of the flood basalts forming the northern Kerguelen Archipelago: Implications for the Kerguelen Plume. *J. Petrol.* **39**, 711–748 (1998).

Yin, Y., Zhang, Q., Zhang, Y., Zhai, S. & Liu, Y. Electrical and thermal conductivity of Earth's core and its thermal evolution—A review. *Acta Geochimica* **41**, 665–688 (2022).

Yoshino, T., Makino, Y., Suzuki, T., & Hirata, T. Grain boundary diffusion of W in lower mantle phase with implications for iso-topic heterogeneity in oceanic island basalts by core-mantle interactions. *Earth Planet. Sci. Lett.* 530, 115887. doi.org/10.1016/j.epsl.2019.115887 (2020).

Zhou, W-Yi, Hao, M., Zhang, J.S., Chen, B., Wang, R., & Schmandt, B. Constraining composition and temperature variations in the mantle transition zone. *Nat. Commun.* **13**. 10.1038/s41467-022-28709-7, (2022).

Zindler, A., Jagoutz, E. & Goldstein, S. Nd, Sr and Pb isotopic systematics in a three-component mantle: a new perspective. *Nature* **298**, 519-523 (1982).

Zindler, A. & Hart, S. Chemical geodynamics. *Ann. Rev. Earth Planet. Sci.* **14**, 493-571 (1986).